APPENDIX A

SOME ASPECTS OF HIGH-PRESSURE PHENOMENA OF BUBBLES IN LIQUIDS AND LIQUID-SOLID SUSPENSIONS

Some aspects of high-pressure phenomena of bubbles in liquids and liquid-solid suspensions

L.-S. Fan, G. Q. Yang, D. J. Lee, K. Tsuchiya, and X. Luo
Department of Chemical Engineering
The Ohio State University
Columbus, Ohio 43210
U.S.A.

ABSTRACT

Some aspects of bubble dynamics and macroscopic hydrodynamic properties in high-pressure bubble columns and three-phase fluidization systems are discussed. Experimental results along with discrete-phase simulations of a single bubble rising in liquids and liquid-solid suspensions at high pressures are presented. A mechanistic model is described, which accounts for the initial size of bubble from a single orifice in liquid-solid suspensions. The mechanism for bubble breakup at high pressures is illustrated by considering bubble instability induced by internal gas circulation inside a bubble, and an analytical expression is obtained to quantify the maximum stable bubble size. Experimental examinations on the roles of bubbles of different sizes indicate the importance of large bubbles in dictating the macroscopic hydrodynamics of slurry bubble columns. Further, extensive studies are made of the key macroscopic hydrodynamic properties, including moving packed bed phenomena, flow regime transition, overall gas holdup, mean bubble size, and bubble size distribution. An empirical correlation is introduced which predicts the gas holdup in slurry bubble columns of different scales. A similarity rule is revealed for the overall hydrodynamics of high-pressure slurry bubble columns, which takes into account the operating conditions, the maximum stable bubble size, and the physical properties of the gas, liquid, and solids. The heat transfer characteristics under high pressures are also investigated. A consecutive film and surface renewal model is used to characterize the heat transfer mechanism.

Keywords — bubble breakup, bubble dynamics, bubble formation, bubble rise velocity, high-pressure three-phase fluidized bed, maximum stable bubble size, slurry bubble column

1. INTRODUCTION

Gas-liquid bubble columns and three-phase fluidization systems are widely used in industry, particularly chemical and petrochemical industries. Three-phase fluidization describes a gas-liquid-solid flow system in which particles are in motion induced by gas and/or liquid phases. Fundamental studies of transport phenomena in bubble columns or three-phase fluidization systems have been extensive over the past decades, and comprehensive reviews are available (Shah *et al.*, 1982; Fan 1989; Deckwer, 1992; Saxena and Chen, 1994). Most studies were conducted under ambient conditions, and relatively little is known regarding high-pressure systems with relevance to industrial processes. Many industrial processes of considerable commercial interest are conducted under high pressures. Examples are: methanol synthesis (at P = 5.5 MPa and T = 0°C), resid hydrotreating (at P = 5.5 to 21 MPa and T = 300 to 425°C), Fischer-Tropsch synthesis (at P = 1.5 to 5.0 MPa and T = 250°C), and benzene hydrogenation (at P = 5.0 MPa and T = 180°C) (Fox, 1990; Jager and Espinoza, 1995; Saxena, 1995; Mill *et al.*, 1996; Peng *et al.*, 1998).

This paper is intended to address the recent advances in transport phenomena of high-pressure bubble columns and three-phase fluidization systems. Selected areas of research centered around the work recently completed by the research group of the senior author at the Ohio State University are discussed together with some relevant works reported in the literature. Experimental results obtained at the Ohio State University are from a high-pressure/high-temperature system of 2- and 4-inch ID columns. The system can be operated at pressures up to 21 MPa and temperatures up to 180°C. Three pairs of windows installed on the column wall allow direct flow visualization to be carried out. Various types of intrusive high-pressure and high-temperature probes, such as the optical fiber probe, and microfoil heat transfer probe, are developed and used to obtain the bubble characteristics and transport properties of the phases. Furthermore, various techniques *via* visualization yield *in-situ* physical properties of the fluids, *e.g.*, the emerging-bubble technique for the surface tension measurement, the hydrostatic weighing method for the density measurement, and the falling-ball technique for the viscosity measurement (Lin and Fan, 1997; Lin *et al.*, 1998).

The selected high-pressure areas discussed in this paper include the bubble

dynamics, covering single bubble rise velocity, bubble formation, and bubble breakup, and the macroscopic hydrodynamic properties, covering moving packed bed phenomena, flow regime transition, overall gas holdup, bubble size, and bubble size distribution, in bubble columns and three-phase fluidized beds. Bubbles rising in liquids and liquid-solid suspensions are examined experimentally as well as numerically. A mechanistic model is described on the bubble formation process from a single orifice in liquid-solid suspensions. The bubble breakup at high pressures is illustrated by considering bubble instability induced by the internal gas circulation inside a bubble, and further, an analytical expression is obtained to quantify the maximum stable bubble size. A correlation is provided to obtain the gas holdup in bubble and slurry bubble columns over a wide range of flow conditions. A similarity rule is revealed for the overall hydrodynamics of high-pressure slurry bubble columns, which takes into account the operating conditions, the maximum stable bubble size, and the physical properties of the gas, liquid, and solids. The heat transfer characteristics are also discussed.

2. BUBBLE DYNAMICS

2.1. Single bubble rise velocity

The characteristics of a rising bubble can be described in terms of the rise velocity, shape and motion of the bubble. These rise characteristics are closely associated with the flow and physical properties (mainly viscosity and presence/absence of solid particles) of the surrounding medium as well as the interfacial properties (*i.e.* presence/absence of surfactant) of the bubble surface. The bubble rise velocity, u_b, is the single most critical parameter in characterizing the hydrodynamics and transport phenomena of bubbles in liquids and liquid-solid suspensions (Fan and Tsuchiya, 1990). The rise velocity of a single gas bubble inherently depends on its size: for small bubbles, the rise velocity strongly depends on liquid properties such as surface tension and viscosity; for large bubbles, the rise velocity is insensitive to liquid properties (Fan, 1989). Under limited conditions, the rise velocities of single bubbles in liquid-solid suspensions were found to be similar to those in highly viscous liquids (Massimilla *et al.*, 1961; Darton and Harrison, 1974). Liquid-solid suspensions can thus be characterized as Newtonian homogeneous media, but they often exhibit non-Newtonian or heterogeneous

behavior (Tsuchiya *et al.*, 1997). Studies in the literature on the bubble rise velocity in liquid-solid suspensions were mainly conducted in water-suspended/fluidized systems and mostly under ambient conditions. Differences in fluidizing media, pressure, and temperature may lead to different bubble rise characteristics.

This section focuses on the bubble rise characteristics in liquids and liquid-solid fluidized beds under frequently encountered industrial conditions, *i.e.* elevated pressure and temperature, and with a non-water based liquid medium. In liquid-solid suspensions under these conditions, the bubble rise velocity is discussed in light of both the apparent homogeneous (or effective) properties of the suspension and the recently evolved numerical prediction based on a computational model for gas-liquid-solid fluidization systems.

2.1.1. In liquids

Krishna *et al.* (1994) studied the pressure effect on the bubble rise velocity and found that the single bubble rise velocity does not depend on the gas density over the range of 0.1 to 30 kg/m^3. The conclusion is limited to a narrow range of pressures. Lin *et al.* (1998) measured the rise velocity of single bubbles of known sizes in Paratherm NF heat transfer fluid at various pressures ranging from 0.1 to 19.4 MPa for three temperatures: 27, 47, and 78°C. The bubble size is represented by the equivalent spherical diameter, d_b. Figure 1 shows their results for (a) 27°C and (b) 78°C. As shown in the figure, for a given bubble size, u_b tends to decrease with increasing pressure at both temperatures. They found that the effects of pressure and temperature, or more directly, the effects of physical properties of the gas and liquid phases on the variation of u_b with d_b could be represented or predicted most generally by the Fan-Tsuchiya equation (Fan and Tsuchiya, 1990) among three predictive equations. The other two are the modified Mendelson's wave-analogy equation (Mendelson, 1967) by Maneri (1995) and a correlation proposed by Tomiyama *et al.* (1995).

The Fan-Tsuchiya equation, generalized for high-pressure systems, can be written in a dimensionless form:

$$u_b' = u_b\left(\frac{\rho_l}{\sigma g}\right)^{1/4} = \left\{\left[\frac{Mo^{-1/4}}{K_b}\left(\frac{\Delta\rho}{\rho_l}\right)^{5/4} d_b'^2\right]^{-n} + \left[\frac{2c}{d_b'} + \left(\frac{\Delta\rho}{\rho_l}\right)\frac{d_b'}{2}\right]^{-n/2}\right\}^{-1/n} \quad (1)$$

where the dimensionless bubble diameter is given by

$$d_b' = d_b(\rho_l g/\sigma)^{1/2}. \quad (2)$$

Three empirical parameters, n, c, and K_b, in Eq. (1) reflect three specific factors governing the rate of bubble rise. They relate to the contamination level of the liquid phase, to the varying dynamic effects of the surface tension, and to the viscous nature of the surrounding medium. The suggested values of these parameters are:

$$n = \begin{cases} 0.8 & \text{for contaminated liquids} \\ 1.6 & \text{for purified liquids} \end{cases}, \quad (3a)$$

$$c = \begin{cases} 1.2 & \text{for monocomponent liquids} \\ 1.4 & \text{for multicomponent liquids} \end{cases}, \text{ and} \quad (3b)$$

$$K_b = \max\left(K_{b0} Mo^{-0.038}, 12\right) \quad (3c)$$

where

$$K_{b0} = \begin{cases} 14.7 & \text{for aqueous solutions} \\ 10.2 & \text{for organic solvents/mixtures} \end{cases}. \quad (3d)$$

The modified Mendelson's equation is a special form of the Fan-Tsuchiya equation where the viscous term, *i.e.* the first term on the right side of Eq. (1), is omitted. Equally general as the Fan-Tsuchiya equation for bubbles in liquids, the correlation by Tomiyama *et al.* (1995), which is given in terms of drag coefficient,

$$C_D = \frac{4}{3}\frac{g\,\Delta\rho\,d_b}{\rho_l u_b^2}, \quad (4)$$

consists of three equations under different system purity:

$$C_D = \max\left\{\min\left[\frac{16}{Re}(1+0.15Re^{0.687}), \frac{48}{Re}\right], \frac{8}{3}\frac{Eo}{Eo+4}\right\} \quad (5a)$$

for purified systems;

$$C_D = \max\left\{\min\left[\frac{24}{Re}(1+0.15Re^{0.687}), \frac{72}{Re}\right], \frac{8}{3}\frac{Eo}{Eo+4}\right\} \quad (5b)$$

for partially contaminated systems; and

$$C_D = \max\left[\frac{24}{Re}(1+0.15Re^{0.687}),\ \frac{8}{3}\frac{Eo}{Eo+4}\right] \tag{5c}$$

for sufficiently contaminated systems. In Eqs (1) and (5), the dimensionless groups are defined as

$$Mo = \frac{g\,\Delta\rho\,\mu_l^4}{\rho_l^2\,\sigma^3}, \tag{6a}$$

$$Re = \frac{d_b u_b \rho_l}{\mu_l}, \text{ and} \tag{6b}$$

$$Eo = \frac{g\,\Delta\rho\,d_b^2}{\sigma} \tag{6c}$$

where $\Delta\rho = \rho_l - \rho_g$. It is noted that u_b can be obtained explicitly from Eq. (1) for a given d_b as well as gas and liquid physical properties, while it can only be obtained implicitly from Eq. (5).

For predictions included in Fig. 1, measured values of physical properties under various operating pressures and temperatures (Lin and Fan, 1997; Lin *et al.*, 1998) are used. As shown in the figure, the modified Mendelson equation, which is valid only under the inviscid condition, provides limited agreement between the measured and calculated results at the low temperature [Fig. 1(a)], suggesting that viscous forces predominate in the bubble rise process. On the other hand, at the high temperature [Fig. 1(b)], there is a strong agreement over the bubble size range of $d_b > 2$ mm including the sharp breakpoint/peak. This indicates that the liquid used tends to behave as a pure inviscid liquid. Note that over the pressure range from 0.1 to 19.4 MPa, the liquid viscosity varies from 29 to 48 mPa·s at 27°C, whereas it is almost constant within a range from 4.7 to 5.2 mPa·s at 78°C (Lin *et al.*, 1998).

The Fan-Tsuchiya equation, Eq. (1), applied for the given liquid, a pure (n = 1.6), multicomponent (c = 1.4) organic solvent (K_{b0} = 10.2), demonstrates good overall predictive capability except for the sharp peak existing for the high-temperature data [Fig. 1(b)]. The equation by Tomiyama *et al.* (1995) also has good general applicability, especially around the peak behavior occurring near d_b = 2 mm at 78°C; however, it tends to underestimate the u_b values over the rest of the d_b range.

The consistent difference in u_b prevailing between 0.1 and 19.4 MPa for $d_b > 2$ mm is due to the significant increase in gas density (as large as 200-fold increase with pressure from 0.1 to 19.4 MPa). The density effect is accounted for in Eq. (1) in terms of $\Delta\rho/\rho_l$ or in Eq. (5) in terms of both $\Delta\rho/\rho_l$ and *Eo*. As can be seen from the equations and figure, the density difference between the continuous liquid phase and the dispersed gas phase plays an important role in determining u_b, especially for large bubbles.

Figure 2 shows the *Re–Eo* relationship often utilized in representing the general rise characteristics of single bubbles in liquids (Clift *et al.*, 1978; Bhaga and Weber, 1981). The thin, background lines signify the general, quantitative trend for the rise velocity of single bubbles in purified Newtonian liquids under ambient conditions, plotted with constant intervals of log *Mo*. The figure shows the general agreement in correlation predictions. The experimental results under four conditions (Lin *et al.*, 1998) are plotted in the figure. By employing accurate values for physical properties of the liquid phase and the gas density at given pressures and temperatures, the experimental results can be successfully represented over the entire *Eo* range, *i.e.* bubble size range, by Eq. (1). The prediction is proven to represent experimental data for various liquids under ambient conditions within some deviations (Tsuchiya *et al.*, 1997). Furthermore, the single bubble rise velocity at high pressures can be reasonably estimated by incorporating the physical properties of the gas and liquid under the operating conditions.

2.1.2. In liquid-solid suspensions

Figure 3 shows the effect of pressure on the bubble rise velocity in a fluidized bed with Paratherm NF heat transfer fluid and 0.88-mm glass beads at (a) 26.5°C and (b) 87.5°C (Luo *et al.*, 1997b). At both temperatures, the bubble rise velocity decreases with an increase in pressure for a given solids holdup. The extent of the reduction is as high as by 50% from 0.1 to 17.3 MPa. A more drastic reduction in u_b, however, arises from the addition of solid particles. While the particle effect is small at low solids holdup ($\varepsilon_s <$ 0.4), the effect is appreciable at high solids holdup (ε_s = 0.545), especially for high liquid viscosity [Fig. 3(a)]. A comparison of the data at 26.5°C and 87.5°C, for the same ε_s of 0.545, indicates that the viscosity effect appears to be significant. The reduction of

the bubble rise velocity with an increase in pressure can lead to a significant increase in the gas holdup of three-phase fluidized beds. The extent of the increase in gas holdup was reported to be around 100% at all gas velocities when the pressure is increased from 0.1 to 15.6 MPa (Luo *et al.*, 1997a). By comparing the pressure effect on the gas holdup with that on the bubble rise velocity, the increase in gas holdup with pressure is a consequence of the decreases in both the bubble size and the bubble rise velocity.

Similar plots are shown in Fig. 4 for the fluidized bed containing 0.21-mm glass beads (Luo *et al.*, 1997b). While the extent of decrease in bubble rise velocity with an increase in pressure is comparable between 0.88- and 0.21-mm glass beads, the extent of decrease in bubble rise velocity with an increase in solids holdup is much smaller for the smaller particles. By comparing the corresponding data in Figs 3 and 4, this difference in the sensitivity of u_b reduction to solids holdup variation is clearly shown for the high solids holdup cases.

The decrease in bubble rise velocity occurs due to corresponding variations of gas and liquid properties with pressure. In the presence of solid particles, it can be assumed, as a first approximation, that the particles modify only homogeneous properties of the surrounding medium. Luo *et al.* (1997b) examined the applicability of this homogeneous approach. The calculated results based on the Fan-Tsuchiya equation, Eq. (1), for u_b are also plotted in Figs 3 and 4, where Eq. (1) is extended to liquid-solid suspensions by replacing the liquid properties, ρ_l and μ_l, by the effective properties of the liquid-solid suspension, ρ_m and μ_m (Tsuchiya *et al.*, 1997), respectively. The effective density can be estimated by

$$\rho_m = \rho_l(1-\varepsilon_s) + \rho_s\varepsilon_s . \tag{7}$$

The calculated results with constant values of μ_m given in Figs 3 and 4 are obtained by coupling Eq. (1) with the following relationship proposed by Tsuchiya *et al.* (1997) for the effective viscosity of liquid-solid suspensions:

$$\frac{\mu_m}{\mu_l} = \exp\left[\frac{K\varepsilon_s}{1-(\varepsilon_s/\varepsilon_{sc})}\right] \tag{8}$$

with two parameters correlated by Luo *et al.* (1997b):

$$K = \frac{3.1 - 1.4 \tanh\left[0.3(10 - 10^2 u_t)\right]}{\phi} \quad \text{and} \tag{9a}$$

$$\varepsilon_{sc} = \left\{1.3 - 0.1 \tanh\left[0.5(10 - 10^2 u_t)\right]\right\} \varepsilon_{s0} \tag{9b}$$

where u_t is in m/s. The ranges of applicability of Eqs (8) and (9) are: $840 < \rho_l < 1000$ kg/m^3; $1 < \mu_l < 47$ mPa·s; $19 < \sigma < 73$ mN/m; $0 < \varepsilon_s < 0.95\,\varepsilon_{s0}$; $7.9\times10^{-4} < u_t < 0.26$ m/s; $0.88 < \phi \leq 1$; and $0.56 < \varepsilon_{s0} < 0.61$.

Equation (1) with parametric values of μ_m, estimated from Eq. (8) under given conditions, predicts reasonably well the general trend exhibited by the reported data. However, a detailed match between the calculated and experimental results appears to be difficult to attain by assigning a constant value of μ_m under each condition. A more elaborate analysis is required to account for the effect of bubble size on interactions of the bubble with the surrounding medium (non-Newtonian approach) or with individual particles (heterogeneous approach).

2.2. Heterogeneous approach: Discrete-phase computation

Jean and Fan (1990) developed a mechanistic model that accounts for impact forces on a rising bubble due to particles. The model can predict the bubble rise velocity for small particles ($d_p < 500$ μm), low-to-intermediate solids holdups ($\varepsilon_s < 0.45$) and large spherical-cap bubbles ($d_b > 15$ mm). It is desired to extend their model to cover the range of smaller bubble sizes as well. This was conducted by Luo *et al.* (1997b) with partial success based on a force balance on a rising bubble involving the net gravity, liquid drag, and particle-bubble collision forces.

A much more thorough scheme of prediction of a single bubble rising in a liquid-solid fluidized bed has recently been developed by Zhang *et al.* (1998b) using a two-dimensional discrete-phase simulation model for gas-liquid-solid fluidization systems. In this model, the volume-averaged method, the dispersed particle method (DPM) and the volume-of-fluid (VOF) method are used to account for the flow of liquid, solid, and gas phases, respectively. A bubble induced force (BIF) model, a continuum surface force (CSF) model, and Newton's third law are applied to account for the couplings of particle-bubble (gas), gas-liquid, and particle-liquid interactions, respectively. A close distance

interaction (CDI) model (Zhang *et al.*, 1998a) is included in the particle-particle collision analysis, which considers the liquid interstitial effects between colliding particles.

2.2.1. Liquid-phase model

The governing equations for the continuous phase of multiphase flows can be derived based on the Navier-Stokes equations for single-phase flows. Considering the existence of dispersed particles, a volume-averaging technique is used to develop a set of partial differential equations to describe the mass and momentum conservation of the liquid phase. The continuity equation for the liquid phase can be given as

$$\frac{\partial \varepsilon_l}{\partial t} + \nabla \cdot (\varepsilon_l v) = 0 . \tag{10}$$

The momentum equation for the liquid phase is

$$\rho_l \frac{\partial (\varepsilon_l v)}{\partial t} + \rho_l \nabla \cdot (\varepsilon_l v v) = -\nabla p + \varepsilon_l \nabla \cdot \tau + \varepsilon_l \rho_l g + f_b \tag{11}$$

where v is the liquid velocity vector, ε_l is the liquid holdup, ρ_l is the liquid density, p is the scalar pressure, τ is the viscous stress tensor, g is the gravitational acceleration, and f_b is the total volumetric body force acting on the liquid phase other than the gravity force.

The Newtonian viscous stress tensor is used which is given as

$$\tau = 2\mu S = \mu \left[(\nabla v) + (\nabla v)^T \right] \tag{12}$$

where S is the rate-of-strain tensor and μ is the coefficient of dynamic viscosity.

2.2.2. Gas-phase model

Under high-pressure conditions, the effects of gas density and viscosity on the flow behavior would be significant. The simulation model for high pressures is conducted by including the simulation of the flow inside the gas bubble. The flow inside the gas bubble is governed by single-phase Navier-Stokes equations. Because of the difficulty of numerical calculation due to the discontinuous jump of properties across the interface between the gas bubble and the liquid-solid suspension, a continuous transition method (CTM) is employed. In this method, the discontinuous characteristics are replaced by a smooth variation of the properties (*e.g.*, density and viscosity) from one phase to another

within the finite interface thickness. The continuous transition method can overcome the problem of numerical divergence while simulating the flow field at both sides of the interface where the physical properties of the fluids strongly differ. By using the high-pressure fluid conditions, the resulting discrete phase simulation method can reveal the pressure effects on the variation of the flow characteristics in a gas-liquid-solid fluidization system.

The scalar fraction function, $\alpha(x, t)$, solved by the VOF method (Hirt and Nichols, 1981) is used to construct this continuous transition function, and the fluid property at the interface can be given by:

$$Q = Q_m^* \alpha(x,t) + Q_g^* [1 - \alpha(x,t)] \tag{13}$$

where Q represents a property of the fluid, Q_m^* and Q_g^* represent the properties of liquid-solid suspension and gas bubble, respectively. By definition, $\alpha(x, t) = 1$ in the liquid or liquid-solid mixture, $0 < \alpha(x, t) < 1$ at the free surface, and $\alpha(x, t) = 0$ in the gas bubble. Therefore, Q is replaced by Q_m^* or Q_g^* when $\alpha(x, t)$ equals 1 in the liquid-solid suspension or equals 0 in the gas bubble.

The advection equation for $\alpha(x, t)$ is

$$\frac{\partial \alpha}{\partial t} + (v \cdot \nabla)\alpha = 0. \tag{14}$$

On the gas-liquid free surfaces, the stress boundary condition follows the Laplace equation as

$$p_s = p - p_v = \sigma\kappa \tag{15}$$

where the surface pressure, p_s, is the surface tension-induced pressure jump across a fluid interface. The continuum surface force (CSF) model (Brackbill *et al.*, 1992) converts the surface force into a volume force within free surfaces. The volume force at the free surfaces is given by the CSF model as

$$f_{sv}(x,t) = \sigma\kappa(x,t)\nabla\alpha(x,t). \tag{16}$$

This volume force is added to the volumetric body force term, f_b, in the momentum equation at the free surfaces.

2.2.3. Dispersed particle method

The motion of a particle in a flow field can be described in Lagrangian coordinates with its origin attached to the center of the moving particle. The motion of a single particle can be described by its acceleration and rotation in a nonuniform flow field. The particle accelerating in the liquid is governed by Newton's second law of motion as

$$m_p \frac{dv_p}{dt} = F_{total} . \tag{17}$$

The forces acting on a particle include interface forces between the fluid and particle, and forces imposed by external fields. The total force acting on a particle is composed of all applicable forces, including drag, added mass, gravity/buoyancy, Magnus force, Basset force, and other forces:

$$F_{total} = F_D + F_{AM} + F_{G/B} + F_{Magnus} + F_{Basset} + \sum_i F_i . \tag{18}$$

The general scheme of a stepwise molecular dynamic (MD) simulation (Allen and Tildesley, 1987), based on a predictor-corrector algorithm, is used to compute the particle motion. The hard sphere approach is used for the collision dynamics. The normal velocity and momentum changes of colliding particles are determined by a collinear collision model developed by Zhang *et al.* (1998a). The model includes the detailed close-range particle-fluid and particle-particle interactions during the entire process of particle collision. The tangential velocity and momentum changes are formulated and calculated based on a sticking/sliding model.

2.2.4. Coupling among individual phases

When particles move into the gas-liquid interface, *i.e.* into the domain where $0.5 < \alpha(x, t) < 1$, the surface tension force is also acting on the particle. This force equals the volumetric surface tension force, f_{sv}, of Eq. (16) multiplied by the particle volume. If the total force of the particle is larger than the surface tension force, the particle would penetrate the bubble surface. The penetrating particle breaks the bubble surface momentarily upon contact. If the penetrating particle is small, the bubble may recover its original shape upon particle penetration (Chen and Fan, 1989). However, if there are several particles colliding with the bubble surface simultaneously, the resulting force may

cause bubble breakage.

Based on Newton's third law of motion, the forces acting on particles from the liquid phase, which include F_D, F_{AM}, and F_{Basset}, yield a reaction force on the liquid. Therefore, the momentum transfer from particles to liquid is taken into account by adding the volumetric liquid-particle interaction force to the body force term, f_b, in Eq. (11).

The liquid properties on the particle surface are obtained by an area-weighted averaging based on the properties at the four grid points of the computational cell containing the particle. The liquid holdup, ε_l, is obtained by subtracting the volume fraction of the particles in the computational cell. However, this cell-averaged liquid holdup is only used for solving the volume-averaged equations of liquid phase. When accounting for the liquid holdup effect on the particle drag coefficient in the liquid-solid medium, a particle-centered area averaging method is used for the calculation.

2.3. Computational results: Single bubble rising

The simulations of representative cases, *i.e.* a single bubble rising and particle entrainment by a bubble in a liquid-solid fluidized bed under ambient conditions (Zhang *et al.*, 1998b), and a single bubble rising in a liquid under high-pressure conditions, are presented in this section.

2.3.1. Ambient conditions

Comparisons of the simulation and the experimental results of a single bubble rising in a liquid-solid suspension are shown in Fig. 5. The simulation domain is 30 × 80 mm^2 and a computational grid size is 0.15 × 0.16 mm^2. One thousand particles with a density of 2,500 kg/m^3 and a diameter of 1.0 mm are used as the solid phase. An aqueous glycerin solution (80 wt%) with ρ_l = 1,206 kg/m^3, μ_l = 52.9 mPa·s, and σ = 62.9 mN/m is used as the liquid phase. A circular bubble with a diameter of 10 mm is initially imposed in the computational domain with its center 15 mm above the bottom. Initially, the particles are randomly positioned in a 30 × 240 mm^2 area. Then, the simulation is performed for particles settling at a liquid velocity of 5 mm/s. At this stage, the bubble is treated as an obstacle and fixed in the original place. An equilibrium bed height is

reached at 80 mm, which gives a three-dimensional equivalent solids holdup of 0.44. After the bed reaches its equilibrium height, the simulation is restarted with bubble tracking and particle movement. The time step of simulation for liquid and solid phases is 5 μs. Experiments are performed in a two-dimensional column with a thickness of 7 mm. The solids holdup, liquid velocity, and the liquid and solids properties are the same as the simulation conditions. As shown in the figure, the simulation and experimental results of the bubble rise velocity and the bubble shape generally agree well.

By closely following the evolution of the particle flow around a single bubble, the mechanisms of particle entrainment in a liquid-solid suspension were studied by Miyahara *et al.* (1989), Fan and Tsuchiya (1990), and Tsuchiya *et al.* (1992). These studies indicated that particles are drawn from the upper surface of the suspension into the freeboard of liquid in the wake behind the bubble, and particle-containing vortices are shed from the wake in the freeboard. The simulation results of the bubble emerging from the bed surface are shown in Fig. 6. As seen in subsequent frames of Fig. 6, a group of particles are dragged by the bubble wake. An agreement in spatial and temporal variations of the solid particles in the entrainment process with the rising bubble is found between the simulation and the experimental results by Miyahara *et al.* (1989) and Tsuchiya *et al.* (1992).

2.3.2. High-pressure conditions

A single bubble rising in a liquid at elevated pressures (P = 19.4 MPa) is simulated. The properties of the liquid phase under ambient conditions are: ρ_l = 868 kg/m^3; μ_l = 29 mPa·s; and σ = 30 mN/m. The computational domain is 100 × 90 mm^2 with 90 × 90 grids. A circular nitrogen bubble with a diameter of 80 mm is initially imposed at 15 mm from the bottom, and its rising behavior is tracked by numerical simulation. The time step of simulation for the liquid and solid phases is 5 μs. Simulation results are shown in Fig. 7, in which the original point of the coordinate system is fixed on the mass center of the rising bubble. The numerical simulation indicates that the bubble rise velocity decreases with an increase in pressure, and is in good agreement with the experimental data and the prediction by the Fan-Tsuchiya equation, Eq. (1). It also can be seen in the figure that the elevated pressure causes the bubble shape to become

more flat due to the variation of properties inside the bubble. As shown in Fig. 7, the simulation cannot only capture the wake structure, but also predict the internal flow circulation structure in the bubble.

2.4. Bubble formation, initial bubble size, and jetting

Numerous experimental and modeling studies have been conducted over the past decades on bubble formation from a single orifice or nozzle submerged in liquids, mostly under ambient conditions (Kupferberg and Jameson, 1969; Kumar and Kuloor, 1970; Azbel, 1981; Lin *et al.*, 1994; Ruzicka *et al.*, 1997). Among various factors that affect the bubble formation, the wettability of the orifice surface is an important factor, which affects the initial size of the bubble formed on the orifice. Lin *et al.* (1994) found that initial bubble size increases significantly with the contact angle between the bubble and the orifice surface when the contact angle exceeds the threshold value of 45°. Various models were established to predict the initial bubble size from a single nozzle in liquids. However, only a few studies were conducted at elevated pressures (LaNauze and Harris, 1974; Idogawa *et al.*, 1987; Tsuge *et al.*, 1992; Wilkinson and Van Dierendonck, 1994). The high-pressure studies indicated that an increase in gas density reduces the size of bubbles formed from a single orifice. However, these results were limited to water systems only. The pressure effect on the initial bubble size in hydrocarbon liquids is not fully understood. Furthermore, studies of the bubble formation in liquids in the presence of particles, as in slurry bubble columns and three-phase fluidized bed systems, are very limited. The experimental data of Massimilla *et al.* (1961) in an air-water-glass beads three-phase fluidized bed revealed that the bubbles formed from a single nozzle in the fluidized bed are larger in size than those in water, and the initial bubble size increases with the solids concentration. Yoo *et al.* (1997) investigated bubble formation in pressurized liquid-solid suspensions. They used 18.6 wt% aqueous glycerol solution and 0.1-mm polystyrene beads as the liquid and solid phases, respectively. The densities of the liquid and the particles were identical, and thus, the particles were neutrally buoyant in the liquid. The results indicated that initial bubble size decreases inversely with pressure under otherwise constant conditions, *i.e.* gas flow rate, temperature, solids concentration, orifice diameter, and gas chamber volume. Their results also showed that

the particle effect on initial bubble size is insignificant. The difference in the finding regarding the particle effects on initial bubble size between Massimilla *et al.* (1961) and Yoo *et al.* (1997) may possibly be due to the difference in particle density.

A mechanistic model is described to predict the initial bubble size in liquid-solid suspensions at high-pressure conditions (Luo *et al.*, 1998c). The model considers various forces induced by the particles, and is an extension of a two-stage spherical bubble formation model developed by Ramakrishnan *et al.* (1969) for liquids. In the two-stage spherical bubble formation model, bubbles are assumed to be formed in two stages, namely, the expansion stage and the detachment stage. The bubble expands with its base attached to the nozzle during the first stage. In the detachment stage, the bubble base moves away from the nozzle, although the bubble remains connected with the nozzle through the neck. The shape of the bubble is assumed to remain spherical during the entire bubble formation process. It is also assumed in this model that a liquid film always exists around the bubble. During the expansion and detachment stages, particles collide with the bubble and stay on the liquid film. The particles and the liquid surrounding the bubble are set in motion as the bubble grows and rises.

The volume of the bubble at the end of the first stage and during the second stage can be described by considering a balance of all the forces acting on the bubble being formed if the instantaneous gas flow rate, Q_o, or the instantaneous gas velocity, u_o, through the orifice, is known. The forces induced by the liquid include the upward forces (effective buoyancy force, F_B, and gas momentum force, F_M), and the downward resistance (liquid drag, F_D, surface tension force, F_σ, bubble inertial force, $F_{I,g}$, and Basset force, F_{Basset}) as shown in Fig. 8. It is assumed that the particles affect the bubble formation process only through two additional downward forces on the bubble, *i.e.* the particle-bubble collision force, F_C, and the suspension inertial force, $F_{I,m}$, due to the acceleration of the liquid and particles surrounding the bubble. Therefore, the overall force balance on the bubble in this model can be written as

$$F_B + F_M = F_D + F_\sigma + F_{Basset} + F_{I,g} + F_C + F_{I,m}. \qquad (19)$$

The expansion stage and the detachment stage follow the same force balance equation, Eq. (19), although the expression for the same force in the two stages may be

different. The expressions for all the forces under two stages are listed in Table 1. The particle-bubble collision force is merely the rate of momentum change of the particles colliding with the bubble surface. The suspension inertial force is calculated from the suspension flow field around an accelerating bubble, obtained from a particle image velocimetry system.

The model is applied to simulate the bubble formation process under constant flow conditions, which are characterized by constant gas flow rate through the orifice. When the volume of the gas chamber is small, the bubble formation can normally be assumed under constant flow conditions. It can be seen from Fig. 9 that the model closely predicts experimental data on the initial bubble size in high-pressure slurry systems (Luo *et al.*, 1998c). Under constant flow conditions ($Nc < 1$), the pressure effect is insignificant. Note that Nc is the dimensionless capacitance number and is equal to $4V_c g\rho_l / \pi D_o^2 P_s$.

In most industrial gas distributors, the gas chamber volume is large and the bubble formation process is under other conditions, *e.g.*, constant pressure or intermediate conditions; in these cases, the orifice gas flow rate is not constant and depends on the pressure fluctuations in the chamber and in the bubble. The experimental study under such conditions is scarce. Yang *et al.* (1999) measured the initial bubble size in a slurry bubble column under intermediate conditions ($Nc > 1$) using an optical fiber probe. As shown in Fig. 10, the pressure has a significant effect on the initial bubble size under these conditions (Yang *et al.*, 1999). The initial bubble size decreases with an increase of pressure for the bubble formation with a large gas chamber. In order to model the bubble formation under such conditions, the pressure fluctuations in the gas chamber and in the bubble must be considered to account for the time-variant orifice gas flow rate as illustrated below.

The instantaneous gas flow rate through the orifice depends on the pressure difference in the gas chamber, P_c, and inside the bubble, P_b, as well as the flow resistance of the orifice, which can be described by the orifice equation as given in Eq. (20a). The pressure in the gas chamber can be evaluated by applying the first law of thermodynamics, considering an adiabatic compression process as given in Eq. (20b) (Wilkinson and Van Dierendonck, 1994). The pressure inside the bubble is governed by a

modified Rayleigh's equation (Pinczewski, 1981). In order to simulate the bubble formation in liquid-solid suspensions, the effect of particles on the pressure inside the bubble must be considered. Yang *et al.* (1999) replaced the liquid inertial term in the modified Rayleigh equation with the suspension inertia, quantified based on the suspension flow field around an accelerating bubble obtained by the PIV measurement, as given in Eq. (20c).

$$\Delta P = \left| P_c - P_b \right| = \left(\frac{Q_o}{k_o} \right)^2 . \tag{20a}$$

$$\frac{\mathrm{d}P_c}{\mathrm{d}t} = \frac{\gamma}{V_c} \left(P_c Q_g - P_c Q_o \right). \tag{20b}$$

$$P_b - P_o = \zeta \rho_m \left[\frac{r_b}{3} \frac{\mathrm{d}^2 r_b}{\mathrm{d}t^2} + \left(\frac{\mathrm{d}r_b}{\mathrm{d}t} \right)^2 \right] + \frac{2\sigma}{r_b} + \frac{4\mu_l}{r_b} \frac{\mathrm{d}r_b}{\mathrm{d}t} . \tag{20c}$$

where p_o is the hydrostatic pressure at the bubble surface. The three terms on the right-hand side of Eq. (20c) represent the contributions of inertial, surface tension, and viscous forces, respectively. The coefficient ζ in Eq. (20c) is equal to 3.86 for bubbles formed in liquid-solid suspensions (Luo *et al.*, 1998c) and to $11/16$ for bubbles formed in liquids, corresponding to the added mass in inviscid liquids (Milne-Thomson, 1955). Combining Eqs (19) and (20a, b, c), and solving these coupled ordinary differential equations simultaneously, the change of the initial bubble size with the time can be obtained. If a certain bubble detachment criterion is used, the initial bubble size can be estimated.

At a low gas velocity, discrete bubbles are formed. On the other hand, at a high gas velocity, jetting occurs and bubbles are formed from the top of the jet. The bubbles formed from a jet are of a wide size distribution. The empirical correlation provided by Idogowa *et al.* (1987) indicated that the bubbling-jetting transition velocity in a liquid is proportional to the gas density raised to the power of -0.8. Luo *et al.* (1998b) investigated the transition from bubbling to jetting under high pressures. They revealed a significant effect of the orifice Reynolds number, $Re_o = \rho_g D_o u_o / \mu_g$, on the bubbling and jetting

phenomena. Photographs of the gas flow through an orifice in Paratherm NF heat transfer fluid at a high pressure for various Re_o are shown in Fig. 11. At Re_o = 1,075, single bubbles are formed from the orifice. With increasing Re_o to 5,321, bubbles being formed at the orifice start to interact with the preceding ones. Bubble coalescence occurs between the two bubbles, sometimes involving more bubbles. At Re_o = 8,809, frequent coalescence of successive bubbles is observed, *i.e.* the beginning of the bubbling-jetting transition. As Re_o increases, the jetting regime becomes more apparent. Bubbles break away from the top of the jet. Moreover, the jet penetration depth increases with an increase in Re_o.

2.5. Bubble coalescence

For gas-liquid systems, the experimental results available in the literature indicate that an increase of pressure retards the bubble coalescence (Sagert and Quinn, 1977, 1978). There are three steps in the bubble coalescence process (Vrij, 1966; Chaudhari and Hoffmann, 1994): (1) approach of two bubbles to form a thin liquid film between them; (2) thinning of the film by the drainage of the liquid under the influence of gravity and suction due to capillary forces; and (3) rupture of the film at a critical thickness. The second step is the rate controlling step in the coalescence process and the bubble coalescence rate can be approximated by the film thinning rate (Vrij, 1966). The film thinning velocity can be expressed as (Sagert and Quinn, 1977, 1978)

$$-\frac{dl}{dt}=\frac{32l^3\sigma}{3\phi R_d^2 \mu_l d_b} \tag{21}$$

where the parameter ϕ is a measure of the surface drag or velocity gradient at the surface due to the adsorbed layer of the gas.

It is known that surface tension decreases and liquid viscosity increases with increasing pressure. In addition, ϕ increases with pressure. As seen from Eq. (21), all these variations contribute to the reduction of the film thinning velocity, and hence, the bubble coalescence rate, as pressure increases. As a result, the time required for two bubbles to coalesce is longer and hence the rate of overall bubble coalescence in the bed is reduced at high pressures. Moreover, the frequency of bubble collision decreases with

increasing pressure. An important mechanism for bubble collision is bubble wake effects (Fan and Tsuchiya, 1990). When the differences in bubble size and bubble rise velocity are small at high pressures, the likelihood of small bubbles being caught and trapped by the wakes of large bubbles decreases. Therefore, bubble coalescence is suppressed by the increase in pressure, due to the longer bubble coalescence time and the smaller bubble collision frequency.

2.6. Bubble breakup and maximum stable bubble size

It is known that the variation of bubble size with pressure is the key to understanding pressure effects on hydrodynamics. The upper limit of the bubble size is set by the maximum stable bubble size, D_{max}, above which the bubble is subjected to breakup and hence is unstable. Several mechanisms have been proposed for the bubble breakup phenomenon and based on these mechanisms, theories have been established to predict the maximum bubble size in gas-liquid systems.

Hinze *et al.* (1955) proposed that the bubble breakup is caused by the dynamic pressure and the shear stresses on the bubble surface induced by different liquid flow patterns, *e.g.*, shear flow and turbulence. When the maximum hydrodynamic force in the liquid is larger than the surface tension force, the bubble disintegrates into smaller bubbles. This mechanism can be quantified by the liquid Weber number. When the Weber number is larger than a critical value, the bubble is not stable and disintegrates. This theory was adopted to predict the breakup of bubbles in gas-liquid systems (Walter and Blanch, 1986). Calculations by Lin *et al.* (1998) showed that the theory underpredicts the maximum bubble size and cannot predict the effect of pressure on bubble size.

A maximum stable bubble size exists for bubbles rising freely in a stagnant liquid without external stresses, *e.g.*, rapid acceleration, shear stress, and/or turbulence fluctuations (Grace *et al.*, 1978). The Rayleigh-Taylor instability has been regarded as the mechanism for bubble breakup under such conditions. A horizontal interface between two stationary fluids is unstable to disturbances with wavelengths exceeding a critical value if the upper fluid has a higher density than the lower one (Bellman and Pennington, 1954):

$$\lambda_c = 2\pi\sqrt{\frac{\sigma}{g(\rho_l - \rho_g)}} \tag{22}$$

Chen and Fan (1988) obtained an equation for a curved surface as in the case of bubble. Grace *et al.* (1978) modified the Rayleigh-Taylor instability theory by considering the time available for the disturbance to grow and the time required for the disturbance to grow to an adequate amplitude. Batchelor (1987) pointed out that the observed size of air bubbles in water was considerably larger than that predicted by the model of Grace *et al.* (1978). Batchelor (1987) further took into account the stabilizing effects of the liquid acceleration along the bubble surface and the non-constant growth rate of the disturbance. In Batchelor's model, the information of the magnitude of the disturbances is required for the prediction of the maximum bubble size; however, the magnitude of the disturbances is not known. The models based on the Rayleigh-Taylor instability predict an almost negligible pressure effect on the maximum bubble size; in fact, Eq. (22) implies that the bubble is more stable when the gas density is higher.

The Kelvin-Helmholtz instability is similar to the Rayleigh-Taylor instability, except that the former allows a relative velocity between the fluids, u_r. Using the same concept of Grace *et al.* (1978), Kitscha and Kocamustafaogullari (1989) applied the Kelvin-Helmholtz instability theory to model the breakup of large bubbles in liquids. Wilkinson and Van Dierendonck (1990) applied the critical wavelength to explain the maximum stable bubble size in high-pressure bubble columns:

$$\lambda_c = \frac{2\pi\sqrt{\dfrac{\sigma}{g(\rho_l - \rho_g)}}}{\dfrac{\rho_l}{\rho_l + \rho_g}\dfrac{\rho_g u_r^2}{2\sqrt{\sigma g(\rho_l - \rho_g)}} + \sqrt{1 + \dfrac{\rho_l^2 \rho_g^2 u_r^4}{4(\rho_l + \rho_g)^2 \sigma g(\rho_l - \rho_g)}}}. \tag{23}$$

Disturbances in the liquid with a wavelength larger than the critical wavelength can break up a bubble. Equation (23) indicates that the critical wavelength decreases with an increase in pressure and therefore bubbles are easier to disintegrate by disturbances at higher pressures. However, the critical wavelength is not equivalent to the maximum stable bubble size, and Eq. (23) alone cannot quantify the effect of pressure on bubble size.

All of the models mentioned above do not account for the internal circulation of the gas. The internal circulation velocity is of the same order of magnitude as the bubble rise velocity. A centrifugal force is induced by this circulation, pointing outwards toward the bubble surface. This force can suppress the disturbances at the gas-liquid interface and thereby stabilizing the interface. The centrifugal force may be another reason to explain the underestimation of D_{max} by the model by Grace *et al.* (1978). On the other hand, the centrifugal force can also disintegrate the bubble, as it increases with an increase in bubble size. The bubble breaks up when the centrifugal force exceeds the surface tension force, especially at high pressures when gas density is high. Levich (1962) assumed the centrifugal force to be equal to the dynamic pressure induced by the gas moving at the bubble rise velocity, *i.e.* $k_f \rho_g u_b^2 / 2$ ($k_f \approx 0.5$), and proposed a simple equation to calculate the maximum stable bubble size:

$$D_{max} \approx \frac{3.63\sigma}{u_b^2 \sqrt[3]{\rho_l^2 \rho_g}}. \tag{24}$$

Equation (24) severely underpredicts the maximum bubble size in air-water systems, although it shows a significant effect of pressure on the maximum bubble size. Considering all the theories proposed in the literature, the mechanism for bubble breakup at high pressures is still unknown.

An analytical criterion for the bubble breakup is derived by considering a single large bubble rising in a stagnant liquid or slurry at a velocity of u_b, without any disturbances on the gas-liquid interface. The bubble is subjected to breakup when its size exceeds the maximum stable bubble size due to the circulation-induced centrifugal force (Luo *et al.*, 1998a). Large bubbles normally assume a spherical cap shape; in this work, the spherical-cap bubble is approximated by an ellipsoidal bubble with the same volume and the same aspect ratio (height to width). The circulation of gas inside the bubble can be described by Hill's vortex (Hill, 1894). To model the bubble breakup, it is necessary to evaluate the x-component of the centrifugal force, F_x, induced by the circulation on the entire bubble surface as shown in Fig. 12. A rigorous theoretical derivation from Hill's vortex yields the expression for F_x:

$$F_x = \frac{9\pi \rho_g u_b^2 a^2}{64\sqrt{2\alpha}}. \tag{25}$$

The surface tension force is the product of the surface tension and the circumference of the bubble,

$$F_\sigma = \sigma L = \sigma \int_{\text{ellipse}} \sqrt{(\delta r_c)^2 + (\delta z)^2} = 4\sigma a \mathrm{E}(\sqrt{1-\alpha^2}). \tag{26}$$

Also, the volume equivalent bubble diameter, d_b, is related to a and α by

$$a = \frac{d_b}{\sqrt[3]{8\alpha}}. \tag{27}$$

Note that the centrifugal force is affected significantly by the gas density, the aspect ratio of the bubble, the bubble size, and the bubble rise velocity. The bubble is not stable if F_x is larger than F_σ, *i.e.*

$$u_b^2 d_b \geq \frac{8\alpha^{4/3} \mathrm{E}(\sqrt{1-\alpha^2})}{0.312} \frac{\sigma}{\rho_g}. \tag{28}$$

When the centrifugal force is larger than the surface tension force, the bubble should be stretched in the x direction. During the stretching, the aspect ratio, α, becomes smaller while d_b and u_b can be assumed to remain constant. As a result, the centrifugal force increases, the surface tension force decreases, and the bubble stretching becomes an irreversible process. The sequence of bubble images shown in Fig. 13 confirms the proposed mechanism of bubble breakup. The bubble images in the figure are obtained at a pressure of 3.5 MPa. Using the Davies-Taylor equation (Davies and Taylor, 1950) for the bubble rise velocity, the maximum stable bubble size is

$$D_{max} \approx 7.16\alpha^{2/3} \mathrm{E}(\sqrt{1-\alpha^2})^{1/2} \sqrt{\frac{\sigma}{g\rho_g}}. \tag{29}$$

The simplified forms of Eq. (29) are (Luo *et al.*, 1998a):

$$D_{max} \approx 2.53 \sqrt{\frac{\sigma}{g\rho_g}} \quad (\text{for } \alpha = 0.21) \tag{30a}$$

in liquids, and

$$D_{max} \approx 3.27\sqrt{\frac{\sigma}{g\rho_g}} \quad (\text{for } \alpha = 0.3) \tag{30b}$$

in liquid-solid suspensions. Further, based on the Davies-Taylor equation, the rise velocity of the maximum stable bubble is

$$u_{max} = C\left(\frac{\sigma g}{\rho_g}\right)^{1/4} \tag{31}$$

where C is a constant. The comparison between experimental data and the predictions of Eq. (30) and by other instability theories is shown in Fig. 14(a). The figure indicates that the proposed model can explain the observed effect of pressure on the bubble size. It is clear that the internal circulation model captures the intrinsic physics of bubble breakup at high pressures. The comparison of the predictions by different models indicates that the bubble breakup is governed by the internal circulation mechanism at high pressures over 10 atm, whereas the Rayleigh-Taylor instability or Kelvin-Helmholtz instability is the dominant mechanism at low pressures. Based on the experimental results at elevated pressures, in which the bubble rise velocity is noted to be proportional to $\rho_g^{-0.5}$, Letzel *et al.* (1998) concluded that the Kelvin-Helmholtz theory governs the bubble instability. However, this proportional relationship between the bubble rise velocity and the gas density should be perceived to be only as a sufficient condition, but not as a necessary condition. This proportional relationship is not necessarily required to be held for a constant square of the growth factor of the disturbance in the Kelvin-Helmholtz theory as the critical wave number may vary with flow conditions under different gas densities. Figure 14(b) presents experimental data and correlation or model predictions of bubble velocity or bubble swarm velocity by various investigators (Davenport *et al.*, 1967; El-Temtamy and Epstein, 1980; Schumpe and Grund, 1986; Wilkinson and Van Dierendonck, 1990; Yu and Kim, 1991; Grund *et al.*, 1992; Wilkinson *et al.*, 1992; Liu and Bankoff, 1993; Hyndman *et al.*, 1997; Letzel *et al.*, 1997, 1998; Luo *et al.*, 1998a) under various operating conditions for air (or nitrogen)-water systems. Relevant information on bubble or bubble swarm velocities in air-water systems regarding these investigations is given in Table 2. It is seen in the figure that bubble or bubble swarm

velocities decrease with an increase in gas density or gas pressure at low gas densities, and this effect is substantially less pronounced at high gas densities. It is found that there is an appreciable variation of the bubble or bubble swarm velocities at low gas densities under various conditions. However at high gas densities, the variation of these velocities appears to be small and these velocities are within the range of prediction of the mechanistic model for high pressures developed by Luo *et al.* (1998a).

3. Macroscopic Hydrodynamics

3.1. Moving packed bed phenomenon

For three-phase fluidization systems involving large particles, two striking phenomena pertaining to macroscopic hydrodynamic behavior are bed contraction and moving packed bed flow. Bed contraction is characterized by a decrease in the bed height of a liquid-solid fluidized bed when a low velocity of gas is introduced to the bed. The bed contraction is caused by the behavior of bubble wake, which entraps liquid and particles and therefore is associated with large bubble systems. The entrainment of the liquid and particles by the bubble wake reduces the effective amount of liquid in the bed used to fluidize the remaining particles. The bed contraction phenomenon has been extensively studied under ambient fluidization conditions (Massimilla *et al.*, 1959; Ostergaard, 1964; El-Temtamy and Epstein, 1979). At high pressures, such a phenomenon has also been observed to occur (Jiang *et al.*, 1997).

The moving packed bed flow is characterized by the motion of solids in piston flow in a three-phase fluidized bed. The moving packed bed flow, which usually occurs during the start-up of the bed, depends not only on the gas and liquid velocities, but also on how they are introduced to the bed. It is caused by the surface phenomena involving fine bubbles attached onto particles and subsequent formation of a fine bubble blanket under the packed solids; a liquid flow would move the entire bed upward. This phenomenon is thus associated with the small bubble system. The moving packed bed flow in a three-phase fluidized bed is a known, anomalous event in the resid hydrotreating industry. It was observed in the 1960s in the bench and pilot units during the development and commercialization of the resid hydrotreating process (Fan, 1999). The reactor was typically operated at pressures between 5.5 and 21 MPa and at

temperatures between 300°C and 425°C. In the early 1970s, the moving packed bed flow was observed in a commercial three-phase fluidized bed reactor. The occurrence of the moving packed bed in a three-phase fluidized bed could simply be circumvented by utilizing a start-up procedure that involves degassing the bed first and then introducing liquid flow to expand the bed prior to commencing the gas flow. Commercial operators of three-phase fluidized bed reactors have long recognized and undertaken a proper start-up procedure of this nature since observing this anomalous event. As the small bubbles can also be generated under the ambient conditions using surfactants in an air-water system, the moving packed bed flow was reported in open literature first by Saberian-Broudjenni *et al.* (1984) and later by Bavarian and Fan (1991a, b) in small columns with small bubbles generated in such manner.

3.2. Flow regime transition

Three flow regimes can be identified based on the bubble flow behavior in bubble columns and slurry bubble columns: the dispersed bubble (or homogeneous bubble flow), the coalesced bubble (or churn-turbulent flow), and the slugging regimes. In the homogeneous bubble flow regime, no bubble coalescence occurs and the bubbles are of uniform, small size. The homogeneous bubble flow regime predominates at high liquid velocities and at low and intermediate gas velocities. At low liquid and high gas velocities, either the churn-turbulent flow or slugging regime occurs depending on the column diameter. In columns of large diameter, the churn-turbulent flow regime always occurs at high gas velocities. In this regime, bubbles tend to coalesce and both bubble size and bubble rise velocity become large and show a wide distribution.

The knowledge of the transition between the homogeneous bubble flow and the churn-turbulent flow regimes is important for the design and operation of industrial reactors. The transition velocity depends on gas distributor design, physical properties of the phases, operating conditions, and column size. The flow regimes and the regime transition have been studied extensively under ambient conditions over the last three decades (Wallis, 1969; Joshi and Lali, 1984; Shnip *et al.*, 1992; Tsuchiya and Nakanishi, 1992; Zahradnik *et al.*, 1997). Most of these studies pointed out a critical role played by the liquid-phase turbulence during the regime transition, and employed

phenomenological models to predict the flow transition from the homogeneous regime to the heterogeneous regime. The effect of the operating pressure on the regime transition has been examined by many researchers in bubble columns (Tarmy *et al.*, 1984; Clark, 1990; Krishna *et al.*, 1991, 1994; Wilkinson *et al.*, 1992; Hoefsloot and Krishna, 1993; Reilly *et al.*, 1994; Letzel *et al.*, 1997; Lin *et al.*, 1999b), in three-phase fluidized beds (Luo *et al.*, 1997a), and in slurry bubble columns (Clark, 1990).

Letzel *et al.* (1997) studied the influence of pressure on the stability of bubbly flows in a bubble column with the nitrogen-water system by using the stability theory of Batchelor (1988) and Lammers and Biesheuvel (1996). They found that a higher gas density has a stabilizing effect on the flow and that the gas fraction at the instability point increases with gas density, while the gas velocity at the instability point only slightly increases with gas density. However, the conclusion is limited to a narrow range of operating pressures (0.1 to 1.3 MPa). Lin *et al.* (1999b) used the standard deviation of the pressure fluctuation and the drift flux model to identify the flow transition from the homogeneous regime to the heterogeneous regime in a bubble column using nitrogen and Paratherm NF heat transfer fluid at pressures up to 15.2 MPa and temperatures up to 78°C. It was found that increasing pressure or temperature delays the regime transition as shown in Fig. 15(a).

Wilkinson *et al.* (1992) proposed a correlation to estimate the gas holdup and gas velocity at the transition point under high-pressure conditions. This predictive scheme incorporates the concept of bimodal bubble size distribution presented by Krishna *et al.* (1991), *i.e.* the churn-turbulent regime is characterized by a bimodal bubble size distribution, consisting of fast rising large bubbles (> 5 cm in diameter) and small bubbles (typically, < 5 mm in diameter). Wilkinson *et al.* (1992) found that the transition velocity depends on the liquid properties and can be estimated by the following correlations:

$$\varepsilon_{g,tran} = \frac{U_{g,tran}}{u_{small}} = 0.5\exp(-193\rho_g^{-0.61}\mu_l^{0.5}\sigma^{0.11}), \text{ and} \tag{32}$$

$$u_{small} = 2.25\left(\frac{\sigma}{\mu_l}\right)\left(\frac{\sigma^3\rho_l}{g\mu_l^4}\right)^{-0.273}\left(\frac{\rho_l}{\rho_g}\right)^{0.03} \tag{33}$$

where u_{small} is the rise velocity of small bubbles. As shown in Fig. 15(a), a reasonable agreement for the regime transition velocity can be obtained between the experimental data obtained by Lin *et al.* (1999b) and the correlation of Wilkinson *et al.* (1992) when the *in-situ* physical properties of the fluids at a given temperature and pressure are used in the correlation.

The studies of the regime transition in three-phase fluidized beds and slurry bubble columns are scarce. Luo *et al.* (1997a) studied the transition velocity in a three-phase fluidized bed over a pressure range of 0.1 to 15.6 MPa by analyzing the drift flux of gas. Two types of glass beads of 2.1 and 3 mm in diameter are used as the solid phase. The drift flux of gas increases with the gas holdup in the dispersed regime; in the coalesced bubble regime, the rate of increase is much larger. As the pressure increases, the transition gas velocity and the gas holdup at the transition point increase, under all the particle size and liquid velocity conditions. The pressure effect on the regime transition is significant, but the effect levels off at a pressure around 6 MPa as shown in Fig. 15(b). The experimental study also shows that the transition velocity increases with liquid velocity and slightly increases with particle size, similar to the regime transition behavior at ambient conditions. Clark (1990) studied the regime transition in a hydrogen-methanol-catalyst system at pressures between 2.5 and 10 MPa and temperatures from 20°C to 180°C. Glass beads with a particle size range of 45 to 63 μm were used as the solid catalyst. It was found that the addition of fine particles to the liquid phase promotes bubble coalescence, which accelerates the transition to the churn-turbulent regime. However, the regime transition at high-pressure conditions in slurry bubble columns is still not fully understood, and further studies are needed to examine the effect of solids concentration on the transition velocity, to develop an accurate correlation, and to explore the transition mechanism.

In general, the pressure effect on the flow regime transition is a result of the variation in bubble characteristics, such as bubble size and bubble size distribution. The bubble size and distribution are closely associated with factors such as initial bubble size, bubble coalescence rates and bubble breakup rates. Under high-pressure conditions, bubble coalescence is suppressed and bubble breakup is enhanced. Also, the distributor tends to generate smaller bubbles. All these factors contribute to small bubble sizes and

narrow bubble size distributions and, consequently, delay the flow regime transition in high-pressure bubble columns and slurry bubble columns.

3.3. Overall gas holdup and hydrodynamic similarity

Gas holdup is a key parameter to characterize the macroscopic hydrodynamics of slurry bubble column systems. The gas holdup depends on gas and liquid velocities, gas distributor design, column geometry (diameter and height), physical properties of the gas and liquid, particle concentration, and physical properties of the particles. The gas holdup generally increases with gas velocity, with a larger rate of increase in the dispersed bubble regime than in the churn-turbulent regime. Such distributors as perforated plate, nozzle injector, and sparger affect the gas holdup significantly only at low gas velocities (Lin *et al.*, 1999a). Lin *et al.* (1999a) also showed that the fluid dynamic behavior of gas and liquid in the plenum region is complex. They observed that the liquid flow in the bottom plenum to the bulk phase of the column through a perforated plate occurs *via* the liquid entrainment mechanism, *i.e.* turbulent gas bubbles and gas circulation in the gas layer entrain liquid from the liquid layer to the distributor as shown in Fig. 16. The gas and liquid flow patterns given in Fig. 16 may characterize, for example, an ebullated bed reactor for resid hydrotreating. In bubble columns, the effect of column size on gas holdup is negligible when the column diameter is larger than 0.1 to 0.15 m (Shah *et al.*, 1982). The influence of the column height is insignificant if the height is above 1 to 3 meters and the ratio of the column height to the diameter is larger than 5 (Kastaneck *et al.*, 1984). Gas holdup decreases as liquid viscosity and/or gas-liquid surface tension increase; however, the effect of liquid density is not clear. The addition of particles into a bubble column leads to a larger bubble size and thus a decreased gas holdup, especially when the particle concentration is low. The particle size effect on the gas holdup can be ignored in the particle size range of 44 to 254 μm.

Numerous studies have been conducted to investigate the effect of pressure on the gas holdup of bubble columns (Deckwer *et al.*, 1980; Tarmy *et al.*, 1984; Idogawa *et al.*, 1986; Kojima *et al.*, 1991; Wilkinson *et al.*, 1992; Reilly *et al.*, 1994; Jiang *et al.*, 1995; Inga, 1997; Letzel *et al.*, 1997; Lin *et al.*, 1998) and three-phase fluidized beds (Luo *et al.*, 1997a). Further, empirical correlations have been proposed for gas holdup in bubble

columns operated at elevated pressure and temperature (Wilkinson *et al.*, 1992; Reilly *et al.*, 1994). It is commonly accepted that elevated pressures lead to a higher gas holdup in both bubble columns and three-phase fluidized beds except in those systems which are operated with porous plate distributors and at low gas velocities. The increased gas holdup is directly related to the smaller bubble size and, to a lesser extent, to the slower bubble rise velocity at higher pressures (Luo *et al.*, 1997b). Figure 17 shows bubbles emerging from the three-phase fluidized bed of Paratherm NF heat transfer fluid and 2.1-mm glass beads over a wide range of operating conditions. As shown in the figure, bubble size is drastically reduced as pressure increases. The most fundamental reason for the bubble size reduction can be attributed to the variation in physical properties of the gas and liquid with pressure.

A significant pressure effect on the gas holdup should exist in slurry bubble columns; however, little is reported concerning such an effect. Deckwer *et al.* (1980) found little effect of pressure on gas holdup in a Fischer-Tropsch slurry bubble column with a porous plate distributor (P = 0.4 to 1.1 MPa; T = 143 to 260°C; U_g = 0 to 3.5 cm/s). The experimental data of Kojima *et al.* (1991) indicated that the gas holdup increases with pressure; but no pressure effect was observed at the 30 wt% solids concentration (P = 0.1 to 1.1 MPa; U_g = 1.7 to 9 cm/s; single orifice distributor). Inga (1997) measured the gas holdup in slurry bubble columns at pressures up to 0.72 MPa and a significant pressure effect was observed. In general, no viable model is available to predict the gas holdup in high-pressure slurry bubble columns. The gas holdup behavior in high-pressure slurry bubble columns is not well understood, especially at high gas velocities.

The dynamic gas disengagement technique, first applied in bubble columns by Sriram and Mann (1977), is utilized to measure the gas holdup in a slurry bubble column under wide operating conditions (Lee *et al.*, 1998). The results obtained with this technique for high-pressure systems are given in Luo *et al.* (1998a). Elevated pressures lead to higher gas holdups in a slurry bubble column. The presence of particles reduces the gas holdup at both ambient and elevated pressures as shown in Fig. 18. An empirical correlation is obtained to estimate the gas holdup in high-pressure slurry bubble columns as

$$\frac{\varepsilon_g}{1-\varepsilon_g} = \frac{2.9\left(\frac{U_g^4 \rho_g}{\sigma g}\right)^{\alpha}\left(\frac{\rho_g}{\rho_m}\right)^{\beta}}{\left[\cosh\left(Mo_m^{0.054}\right)\right]^{4.1}} \tag{34}$$

where Mo_m is the modified Morton number for the slurry phase, $g(\rho_m - \rho_g)(\xi \mu_l)^4 / \rho_m^2 \sigma^3$, and

$$\alpha = 0.21 Mo_m^{0.0079} \tag{35a}$$

$$\beta = 0.096 Mo_m^{-0.011}. \tag{35b}$$

A correction factor ξ accounts for the effect of particles on the slurry viscosity:

$$\ln \xi = 4.6\varepsilon_s \left\{5.7\varepsilon_s^{0.58} \sinh\left[-0.71\exp(-5.8\varepsilon_s)\ln(Mo)^{0.22}\right] + 1\right\} . \tag{36}$$

Table 3 lists the various experimental systems and their corresponding references used to obtain the correlation. The average error of the predictions is 13% for both the slurry and gas-liquid systems and the maximum error is 53%. The applicable ranges of the correlation are summarized in Table 4.

The physical meaning of the dimensionless group of $U_g^4 \rho_g / \sigma g$ in Eq. (34) can be shown by substituting Eq. (31) into the group:

$$\frac{U_g^4 \rho_g}{\sigma g} \propto \left(\frac{U_g}{u_{max}}\right)^4 \tag{37}$$

Clearly, the dimensionless group represents the contribution of large bubbles to the overall gas holdup, which is the major reason why the correlation can cover such wide ranges of experimental conditions.

For high-pressure bubble columns and slurry bubble columns operated under the wide range of conditions outlined in Table 3, hydrodynamic similarity requires the following dimensionless groups to be the same: U_g / u_{max}, Mo_m, and ρ_g / ρ_m. To simulate the hydrodynamics of industrial reactors, cold models can be used and milder pressure and temperature conditions can be chosen, as long as the three groups are similar to those in the industrial reactor. The similarity rule needs to be tested in industrial reactors.

3.4. Bubble size distribution and dominance of large bubbles

The bubble size can be measured by photographic or probe techniques. In multi-bubble systems, a mean bubble size is usually used to describe the system. The mean bubble size is commonly expressed through the Sauter, or volume-surface, mean. For a group of bubbles with measured diameters, the Sauter mean is

$$d_{vs} = \frac{\sum n_i d_{bi}^3}{\sum n_i d_{bi}^2} \tag{38}$$

where n_i is the number of bubbles in the class i with its volume equivalent size d_{bi}.

Some studies have been conducted to investigate pressure or gas density effects on mean bubble size and bubble size distribution in bubble columns (Idogawa *et al.*, 1986, 1987; Jiang *et al.*, 1995; Soong *et al.*, 1997; Lin *et al.*, 1998) as well as in three-phase fluidized beds (Jiang *et al.*, 1992, 1997). According to these experimental studies, pressure has a significant effect on mean bubble diameter. The mean bubble diameter decreases with increasing pressure; however, above a certain pressure, the bubble size reduction is not significant. The effect of pressure on the mean bubble size is due to the change of bubble size distribution with pressure. At atmospheric pressure, the bubble size distribution is broad, while under high pressure, the bubble size distribution becomes narrower and is in smaller size ranges as shown in Fig. 19 (Luo *et al.*, 1998a). At ambient conditions and U_g = 38.5 cm/s, the slurry bubble column is in the slugging regime with the maximum bubble size of 7.2 cm, approximately. At P = 5.6 MPa, bubble size is much smaller and slugs are not observed even at U_g = 37.4 cm/s. According to the literature, bubble size is affected by bubble formation at gas distributor, bubble coalescence and bubble breakup. When the pressure is increased, the bubble size at the distributor is reduced (Luo *et al.*, 1998c), bubble coalescence is suppressed (Jiang *et al.*, 1995), and large bubbles tend to breakup, *i.e.* the maximum stable bubble size is reduced (Luo *et al.*, 1998a). The combination of these three factors causes the decrease of mean bubble size with increasing pressure.

The bubble size distribution can normally be approximated by a log-normal distribution with its upper limit at the maximum stable bubble size. The contribution of bubbles of different sizes can be examined by analyzing the relationship between overall

gas holdup and bubble size distribution. In slurry bubble columns, the gas holdup can be related to the superficial gas velocity, U_g, and the average bubble rise velocity, $\overline{u}_b$, (based on bubble volume) by a simple equation:

$$U_g = \varepsilon_g \overline{u}_b . \tag{39}$$

When the distributions of bubble size and bubble rise velocity are taken into account, $\overline{u}_b$ can be expressed as

$$\overline{u}_b = \frac{\int_{d_{b,min}}^{d_{b,max}} V_b(d_b) f(d_b) u_b(d_b) \mathrm{d}d_b}{\int_{d_{b,min}}^{d_{b,max}} V_b(d_b) f(d_b) \mathrm{d}d_b} . \tag{40}$$

The outcome of Eq. (40) and the gas holdup strongly depend on the existence of large bubbles, because of the large volume and high rise velocity of such large bubbles. An experimental study by Lee *et al.* (1998) revealed that, in the coalesced bubble regime, more than 70% of the small bubbles are entrained by the wakes of large bubbles and consequently have a velocity close to that of large bubbles. It is clear that the large bubbles have a dominant effect on the overall hydrodynamics of slurry bubble columns due to their large volume, their high rise velocity, and the wakes associated with the large bubbles.

3.5. Heat transfer characteristics

Studies reported in the literature for heat transfer characteristics in slurry bubble columns (Saxena *et al.*, 1990; Li and Prakash, 1997) have been limited to ambient conditions. Little has been reported for high-pressure conditions. Since heat transfer behavior is closely associated with macroscopic flow structures and microscopic flow characteristics, a variation in pressure, which alters the physical properties of the gas and liquid, and also affects the hydrodynamics, would yield a complex effect on heat transfer behavior in the system. Previous studies on heat transfer in three-phase fluidized beds with liquids of different viscosity indicates that liquid viscosity has a negative effect on heat transfer (Kato *et al.*, 1981; Kang *et al.*, 1985). Since liquid viscosity increases with pressure, pressure would have a negative effect on heat transfer. Other physical properties

of liquid, which are less affected by pressure, include liquid density, ρ_l, liquid thermal conductivity, k_l, and liquid heat capacity, C_{pl} (Reid *et al.*, 1977).

Studies on instantaneous heat transfer in liquids and liquid-solid systems which involve the injection of single bubbles revealed the importance of bubble wakes to heat transfer behavior (Kumar *et al.*, 1992). The heat transfer enhancement by bubbles increases with bubble size due to the increased wake size and wake vortical intensity. When the pressure increases, the bubble size decreases, and hence the wake contribution to the heat transfer by single bubbles is reduced. In chain bubbling systems, Kumar and Fan (1994) reported that the time-averaged heat transfer coefficient increases with bubbling frequency due to the intense bubble-wake, bubble-bubble, and bubble-surface interactions. The effect of pressure on heat transfer due to the variations in liquid properties and hydrodynamic parameters is summarized in Table 5. The overall effect of pressure on heat transfer behavior depends on the outcome of the counteracting effects of each individual factor.

Deckwer *et al.* (1980) measured the heat transfer coefficient from an immersed heat source to the surrounding gas-liquid or gas-liquid-solid systems under conditions which prevail the Fischer-Tropsch slurry process (P = 0.1 to 1.0 MPa; T = 250 to 300°C; 16 wt% of 5 μm particles). Based on the surface renewal model and Kolmogoroff's theory of isotropic turbulence, a correlation was obtained to predict the heat transfer coefficient in slurry bubble columns:

$$St = 0.1\left(Re\ Fr\ Pr^2\right)^{-0.25}. \tag{41}$$

In the model, the liquid-solid suspension was considered as a homogeneous phase, and consequently, the estimation scheme of the physical properties of the suspension from the individual phase was required.

Luo *et al.* (1997a) studied the heat transfer behavior in a three-phase fluidized bed over a pressure range of 0.1 to 15.6 MPa. Two types of glass beads, 2.1 and 3 mm in diameter, were used as the solid phase. The effects of gas velocity and pressure on the heat transfer coefficient are shown in Fig. 20. With an increase in pressure, the heat transfer coefficient increases, reaches a maximum at pressures of 6 to 8 MPa, and then decreases. An empirical equation is proposed to correlate the experimental data in their

study:

$$h = h'\varepsilon_g^{0.45}\left(\frac{0.396}{U_g^{0.45}} + \frac{0.6768}{u_{pt,0}}\right) \tag{42}$$

where h' is the heat transfer coefficient of a liquid-solid fluidized bed with the same solids holdup, and $u_{pt,0}$ is the particle terminal velocity in the fluidizing liquid at ambient pressure. In Eq. (42), the units for U_g and $u_{pt,0}$ are in m/s. The heat transfer coefficient, h', can be calculated by the correlation given below (Richardson *et al.*, 1976):

$$Nu' = 0.67 Re^{0.62} Pr^{0.33} \frac{\varepsilon_s^{0.38}}{1-\varepsilon_s}. \tag{43}$$

The average deviation of the prediction from the experimental data is within ±10%.

Yang *et al.* (1998) studied heat transfer between an immersed solid surface and bulk fluids in a slurry bubble column at pressures of 0.1 to 6.3 MPa and temperatures of 35 to 81°C. Glass beads of 50 μm in diameter are used as the solid phase. The solids concentrations are varied up to 35 vol%, while the superficial gas velocities are varied up to 20 cm/s. The pressure effect on the heat transfer coefficient is shown in Fig. 21. It is found that pressure has a significant effect on the heat transfer characteristics in a slurry bubble column. The heat transfer coefficient decreases appreciably with increasing pressure except under very high pressures. The variation of the heat transfer coefficient with pressure is attributed to the counteracting effects of the variations of liquid viscosity, bubble size and bubbling frequency with pressure. When pressure increases, bubble size decreases; however, the bubbling frequency increases, which augments the rate of heat transfer (Kumar and Fan, 1994). The counteracting effects of the above two factors give rise to the overall effect of pressure on the heat transfer rate. In a slurry bubble column, pressure reduces bubble size significantly at pressures lower than 4 MPa, which results in the decrease of heat transfer coefficient. When the pressure is further increased, the bubble size reduction is relatively smaller, and the increase in bubbling frequency contributes to an increase in the heat transfer coefficient. However, in a three-phase fluidized bed, due to the large particle size, the bubble size reduction becomes a less important factor in affecting the heat transfer coefficient, and the heat transfer coefficient increases with the increase of bubbling frequency.

A consecutive film and surface renewal model originally developed by Wasan and Ahluwalia (1969) may be used to analyze the heat transfer behavior. The model assumes that a thin liquid film with a thickness of δ exists surrounding the heating surface; and liquid elements are forced to contact the outer surface of the film, due to the passage of bubbles. The liquid elements contact the film for a short time, t_c, and then, are replaced by fresh liquid elements. The heat is transferred to the bulk liquid through conduction by the liquid film and unsteady state conduction by the liquid elements. The heat transfer coefficient is expressed in terms of the physical properties of the liquid, the film thickness, and the contact time of the liquid elements (Wasan and Ahluwalia, 1969):

$$h = \frac{2k_l}{\sqrt{\pi\alpha t_c}} + \frac{k_l\delta}{\alpha t_c}\left[e^{\alpha t_c/\delta^2}\left(1-\operatorname{erf}\frac{\sqrt{\alpha t_c}}{\delta}\right)-1\right] \tag{44}$$

Based on Eq. (44), the heat transfer coefficient is a function of film thickness and contact time between the liquid element and film. The order of magnitude of the film thickness may be estimated by (Kumar and Fan, 1994)

$$\delta = \frac{6.14L}{Re_m^{3/4}} Pr^{-1/3} \tag{45}$$

where Re_m is equal to $\rho_m L u_b/\mu_m$. Assuming that the element contact time is equal to the bubble contact time with the film, the contact time can be estimated from (Kumar and Fan, 1994)

$$t_c = \frac{L}{u_b} \tag{46}$$

where u_b is the actual bubble rise velocity in a stream of bubbles. By considering the pressure effects on the physical properties of liquid and bubble characteristics, such as bubble size and bubble rise velocity, this model may be used to analyze the heat transfer behavior in a high-pressure system.

4. CONCLUDING REMARKS

Experimental results show the rise velocity of single bubbles in liquids and liquid-solid suspensions decreases with an increase in pressure and with a decrease in temperature. This decrease, combined with the pressure effect of reducing the bubble size, contributes to high gas holdups observed at high pressures. The bubble rise velocity

in liquids and liquid-solid suspensions with low solids holdups can be reasonably estimated by use of the predictive equation available for ambient conditions, if the *in-situ* physical properties of the gas and liquid are used. Significant reduction in the rise velocity occurs at high solids holdups, especially for high liquid viscosity. The extent of reduction can be examined in terms of an increase in the apparent suspension viscosity by applying the homogeneous, Newtonian analogy. Along with the experimental results, discrete-phase simulations of a single bubble rising in liquid-solid suspensions at ambient conditions and in liquids at an elevated pressure are presented. A mechanistic model is described which accounts for the initial bubble size from a single orifice in liquid-solid suspensions. The mechanistic analysis indicates that the heterogeneous characteristics of liquid-solid suspensions can be satisfactorily accounted for by considering the particle-bubble collision behavior. The proposed mechanistic model successfully predicts the initial bubble size from a single orifice in high-pressure liquid-solid suspensions. The mechanism for bubble breakup at high pressures is illustrated by considering the bubble instability induced by internal gas circulation inside a bubble, and an analytical expression is obtained to quantify the maximum stable bubble size. Theoretical and experimental examinations on the roles of bubbles of different sizes indicate the important role that large bubbles play in dictating the macroscopic hydrodynamics of slurry bubble columns. An empirical correlation is provided to predict the gas holdup in slurry bubble columns over a wide range of conditions. A similarity rule is revealed for the overall hydrodynamics of high-pressure slurry bubble columns, which takes into account the operating conditions, the maximum stable bubble size, and the physical properties of the gas, liquid, and solids. A consecutive film and surface renewal model is used to explore the heat transfer characteristics in high-pressure three-phase fluidized beds and slurry bubble columns.

5. acknowledgement

This work was supported by the National Science Foundation Grant CTS-9528380, the U.S. Department of Energy Grant DEFC22-95 PC 95051 with Cooperative Agreement with Air Products and Chemicals, Inc., and the Ohio State University / Industry Consortium Program on Fluidization and Multiphase Flow.

6. NOTATION

a	half x-axis length in Fig. 12
C	constant in Eq. (31)
C_D	drag coefficient
C_{pl}	liquid heat capacity
c	parameter in Eq. (1) reflecting surface tension effect
D_c	column diameter
D_{max}	maximum stable bubble size
D_o	orifice diameter
d_b	volume equivalent bubble diameter
d_b'	dimensionless bubble diameter
d_p	particle diameter
d_{vs}	Sauter mean bubble diameter
$\mathrm{E}\left(\sqrt{1-\alpha^2}\right)$	complete second kind Elliptic integral
Eo	Eötvös number
e	restitution coefficient
F_{AM}	added mass force
F_B	buoyancy force
F_{Basset}	Basset force
F_c	particle-bubble collision force
F_D	liquid drag force
$F_{G/B}$	gravity/buoyancy force
$F_{I,g}$	bubble inertial force
$F_{I,m}$	liquid-solid suspension inertial force
F_M	gas momentum force
F_{Magnus}	Magnus force
F_{total}	total force

F_x	x-component of centrifugal force induced by internal circulation
F_σ	surface tension force
Fr	Froude number
f_b	volumetric body force
f_{sv}	volume force within free surface
$f(d_b)$	probability density function of bubble size
g	gravitational acceleration
H	column height
h	time-averaged heat transfer coefficient
h'	heat transfer coefficient in liquid-solid fluidized beds
K	proportionality constant defined by Eq. (9a)
K_b	parameter in Eq. (1) reflecting viscous nature of surrounding medium
K_{b0}	proportionality constant defined by Eq. (3d)
k_l	liquid thermal conductivity
k_o	orifice constant
L	circumference of the ellipse
	length of the heat transfer probe
l	thickness of the liquid film between two coalescing bubbles
Mo	Morton number
Mo_m	modified Morton number based on slurry properties
m_p	particle mass
Nc	dimensionless capacitance number
Nu'	Nusselt number in liquid-solid fluidized beds
n	parameter in Eq. (1) reflecting system purity
n_i	number of bubbles
P	pressure
P_b	pressure in the bubble
P_c	pressure in the gas chamber
P_e	pressure at the gas inlet to the chamber

P_o	hydrostatic pressure at the bubble surface
P_s	system pressure
Pr	Prandtl number
p_s	surface pressure
Q	property of fluid in Eq. (13)
Q_g^*	property of gas
Q_m^*	property of liquid-solid suspension
Q_o	volumetric gas flow-rate through the orifice
Q_g	volumetric gas flow-rate into the gas chamber
R_d	radius of a contacting circle between two bubbles
Re	bubble Reynolds number based on liquid properties
Re_m	bubble Reynolds number based on slurry properties
Re_o	orifice Reynolds number
r_b	radius of bubble
r_c	radius in a cylindrical coordinate system
r_o	radius of orifice
S	rate-of-strain stress
St	Stanton number
T	temperature
t	time
t_c	contact time between liquid element and film
U_g	superficial gas velocity
$U_{g,tran}$	transition gas velocity
U_l	superficial liquid velocity
u	rise velocity of bubble base
u_b	bubble rise velocity relative to the liquid phase
	absolute bubble rise velocity in a stream of bubble in Eq. (46)
u_b'	dimensionless bubble rise velocity defined by Eq. (1)

$\overline{u}_b$	average bubble rise velocity
u_e	bubble expansion velocity
u_{large}	large bubble rise velocity
u_m	suspension velocity
u_{max}	rise velocity of maximum stable bubble
u_o	superficial gas velocity through the orifice
$u_{pt,0}$	particle terminal velocity in the fluidizing liquid at the ambient pressure
u_r	relative velocity between liquid and gas inside a bubble
u_{small}	small bubble rise velocity
u_{swarm}	bubble swarm velocity
u_t	particle terminal velocity in liquid
V_c	volume of gas chamber
$\boldsymbol{v}$	liquid velocity vector
$\boldsymbol{v}_p$	particle velocity vector
z	z-axis in a cylindrical coordinate system

Greek letters

α	aspect ratio of bubble
	scalar field function in Eq. (13)
	thermal diffusivity
δ	thickness of liquid film
ε_g	gas holdup
$\varepsilon_{g,tran}$	gas holdup at the transition point
ε_l	liquid holdup
ε_s	solids holdup
ε_{sc}	critical solids holdup
ε_{s0}	solids holdup at incipient fluidization
ϕ	particle sphericity

	parameter in Eq. (21) reflecting the surface drag
γ	heat capacity ratio
	contact angle
κ	free surface curvature
λ_c	critical wavelength
μ	coefficient of dynamic viscosity
μ_g	gas viscosity
μ_l	liquid viscosity
μ_m	(effective) viscosity of liquid-solid suspension
ρ_g	gas density
ρ_l	liquid density
ρ_m	density of liquid-solid suspension
ρ_s	solids density
σ	surface tension
τ	viscous stress tensor
ξ	correction factor defined by Eq. (36)
ζ	coefficient in Eq. (20c)

7. REFERENCES

Akita, K. and F. Yoshida, 1973. Gas holdup and volumetric mass transfer coefficient in bubble columns. *Ind. Eng. Chem. Process Des. Develop.*, **12**, 76.

Allen, M. P. and D. J. Tildesley, 1987. *Computer Simulation of Liquids*, Clarendon Press, Oxford.

Azbel, D., 1981. *Two-Phase Flows in Chemical Engineering*, Cambridge Univ. Press, Cambridge, UK.

Bach, H. F. and T. Pilhofer, 1978. Variation of gas hold-up in bubble columns with physical properties of liquids and operating parameters of columns. *Ger. Chem. Eng.*, **1**, 270.

Batchelor, G. K., 1987. The stability of a large gas bubble rising through liquid. *J. Fluid Mech.*, **184**, 399.

Batchelor, G. K., 1988. A new theory of the instability of a uniform fluidized bed. *J. Fluid Mech.*, **193**, 75.

Bavarian, F., and L.-S. Fan, 1991a. Mechanisms of hydraulic transport of a packed bed at the start-up of a three-phase fluidized bed. *Chem. Eng. Sci.*, **46**, 3081.

Bavarian, F., and L.-S. Fan, 1991b. Hydraulic transport of a packed bed during the start-up of a three-phase fluidized bed with large gas holdups. *Ind. Eng. Chem. Res.*, **30**, 408.

Bellman, R. and R. H. Pennington, 1954. Effect of surface tension and viscosity on Taylor instability. *Q. Appl. Math.*, **51**, 151.

Bhaga, D. and M. E. Weber, 1981. Bubbles in viscous liquids: shapes, wakes, and velocities. *J. Fluid Mech.*, **105**, 61.

Brackbill, J. U., D. B. Kothe, and C. Zemach, 1992. A continuum method for modeling surface tension. *J. Comp. Phys.*, **100**, 335.

Chaudhari, R. V. and H. Hoffmann, 1994. Coalescence of gas bubbles in liquids. *Rev. Chem. Eng.*, **10**, 131.

Chen, Y.-M. and L.-S. Fan, 1988. On the criteria of Rayleigh-Taylor instability at a curved interface by a local force balance. Unpublished work.

Chen, Y.-M. and L.-S. Fan, 1989. Bubble breakage due to particle collision in a liquid medium. *Chem. Eng. Sci.*, **44**, 2762.

Clark, K. N., 1990. The effect of high pressure and temperature on phase distributions in a bubble column. *Chem. Eng. Sci.*, **45**, 2301.

Clift, R., J. R. Grace, and M. E. Weber, 1978. *Bubbles, Drops, and Particles*. Academic Press, New York.

Darton, R. C. and D. Harrison, 1974. The rise of single gas bubbles in liquid fluidized beds. *Trans. Instn Chem. Engrs*, **52**, 301.

Davenport, W. G., F. D. Richardson, and A. V. Bradshaw, 1967. Spherical cap bubbles in low density liquids. *Chem. Eng. Sci.*, **22**, 1221.

Davies, R. M. and G. I. Taylor, 1950. The mechanics of large bubbles rising through extended liquids and through liquids in tubes. *Proc. Roy. Soc. London*, **A200**, 375.

Deckwer, W.-D., 1992. *Bubble Column Reactors*, John Wiley and Sons, Chichester, England.

Deckwer, W.-D., Y. Louisi, A. Zaidi, and M. Ralek, 1980. Hydrodynamic properties of the Fischer-Tropsch slurry process. *Ind. Eng. Chem. Process Des. Dev.*, **19**, 699.

El-Temtamy, S. A. and N. Epstein, 1979. Contraction of expansion of three-phase fluidized beds containing fine/light solids. *Can. J. Chem. Eng.*, **57**, 520.

El-Temtamy, S. A. and N. Epstein, 1980. Rise velocities of large single two-dimensional and three-dimensional gas bubbles in liquids and in liquid fluidized beds. *Chem. Eng. J.*, **19**, 153.

Fan, L.-S., 1989. *Gas-Liquid-Solid Fluidization Engineering*, Butterworths, Stoneham, MA.

Fan, L.-S., 1999. Moving packed bed phenomena in three-phase fluidization. *Powder Technology*, in press.

Fan, L.-S. and K. Tsuchiya, 1990. *Bubble Wake Dynamics in Liquids and Liquid-Solid Suspensions*. Butterworth-Heinemann, Stoneham, MA.

Fox, J. M., 1990. Fischer-Tropsch reactor selection. *Catal. Lett.*, **7**, 281.

Grace, J. R., T. Wairegi, and J. Brophy, 1978. Break-up of drops and bubbles in stagnant media. *Can. J. Chem. Eng.*, **56**, 3.

Grund, G., A. Schumpe, and W.-D. Deckwer, 1992. Gas-liquid mass transfer in a bubble column with organic liquids. *Chem. Eng. Sci.*, **47**, 3509.

Hill, M. J. M., 1894. On a spherical vortex. *Phil. Trans. Roy. Soc. London*, **185**, 213.

Hinze, J. O., 1955. Fundamentals of the hydrodynamic mechanism of splitting in dispersion processes. *AIChE J.*, **1**, 289.

Hirt, C. W. and B. D. Nichols, 1981. Volume of fluid (VOF) method for the dynamics of free boundaries, *J. Comp. Phys.*, **39**, 201.

Hoefsloot, H. C. J. and R. Krishna, 1993. Influence of gas density on the stability of homogeneous flow in bubble columns. *Ind. Eng. Chem. Res.*, **32**, 747.

Hyndman, C. L., F. Larachi, and C. Guy, 1997. Understanding gas-phase hydrodynamics in bubble columns: A convective model based on kinetic theory. *Chem. Eng. Sci.*, **52**, 63.

Idogawa, K., K. Ikeda, T. Fukuda, and S. Morooka, 1986. Behavior of bubbles of the air-water system in a column under high pressure. *Int. Chem. Eng.*, **26**, 468.

Idogawa, K., K. Ikeda, T. Fukuda, and S. Morooka, 1987. Formation and flow of gas bubbles in a single orifice or nozzle gas distributor. *Chem. Eng. Comm.*, **59**, 201.

Inga, J. R., 1997. Scaleup and scaledown of slurry reactors: a new methodology. *Ph.D. thesis*, University of Pittsburgh, PA.

Jager, B. and R. Espinoza, 1995. Advances in low temperature Fischer-Tropsch synthesis. *Catal. Today*, **23**, 17.

Jean, R.-H. and L.-S. Fan, 1990. Rise velocity and gas-liquid mass transfer of a single large bubble in liquids and liquid-solid fluidized beds. *Chem. Eng. Sci.*, **45**, 1057.

Jiang, P., D. Arters, and L.-S. Fan, 1992. Pressure effects on the hydrodynamic behavior of gas-liquid-solid fluidized beds. *Ind. Eng. Chem. Res.*, **31**, 2322.

Jiang, P., T.-J. Lin, X. Luo, and L.-S. Fan, 1995. Visualization of high pressure (21 MPa) bubble column: bubble characteristics. *Chem. Eng. Res. & Des.*, **73**, 269.

Jiang, P., X. Luo, T.-J. Lin, and L.-S. Fan, 1997. High temperature and high pressure three-phase fluidization—bed expansion phenomena. *Powder Technology*, **90**, 103.

Joshi, J. B. and A. M. Lali, 1984. Velocity-hold up relationship in multiphase contactors-a unified approach. *Frontiers in Chem. Reaction Eng.*, **1**, 314, Wiley Eastern, New York.

Kang, Y., I. S. Suh, and S. D. Kim, 1985. Heat transfer characteristics of three-phase fluidized beds. *Chem. Eng. Comm.*, **34**, 1.

Kastaneck, F., J. Zahradnik, J. Kratochvil, and J. Cermak, 1984. Modelling of large-scale bubble column reactors for non-ideal gas-liquid systems in *Frontiers in Chemical Reaction Engineering*, edited by L. K. Doraiswamy and R. A. Mashelkar, **1**, 330, Whiley, Bombay, India.

Kato, Y., K. Uchida, and S. Morooka, 1981. Liquid holdup and heat transfer coefficient between bed and wall in liquid-solid and gas-liquid-solid fluidized beds. *Powder Technology*, **28**, 173.

Kitscha, J. and G. Kocamustafaogullari, 1989. Breakup criteria for fluid particles. *Int. J. Multiphase Flow*, **15**, 573.

Koide, K., A. Takazawa, and M. Komura, 1984. Gas Holdup and Volumetric Liquid-Phase Mass Transfer Coefficient in Solid-Suspended Bubble Columns. *J. Chem. Engng. Japan*, **17**, 459.

Kojima, H., B. Okumura, and A. Nakamura, 1991. Effect of pressure on gas holdup in a bubble column and a slurry bubble column. *J. Chem. Engng. Japan*, **24**, 115.

Krishna, R., J. W. A. De Swart, D. E. Hennephof, J. Ellenberger, and C. J. Hoefsloot, 1994. Influence of increased gas density on hydrodynamics of bubble-column reactors. *AIChE J.*, **40**, 112.

Krishna, R., P. M. Wilkinson, and L. L. Van Dierendonck, 1991. A model for gas holdup in bubble columns incorporating the influence of gas density on flow regime transitions. *Chem. Eng. Sci.*, **46**, 2491.

Kumar, R. and N. R. Kuloor, 1970. The formation of bubbles and drops. *Advances in Chemical Engineering*, **8**, 255.

Kumar, S., K. Kusakabe, K. Raghunathan, and L.-S. Fan, 1992. Mechanism of heat transfer in bubbly liquid and liquid-solid systems: single bubble injection. *AIChE J.*, **38**, 733.

Kumar, S. and L.-S. Fan, 1994. Heat-transfer characteristics in viscous gas-liquid and gas-liquid-solid systems. *AIChE J.*, **40**, 745.

Kupferberg, A. and G. J. Jameson, 1969. Bubble formation at a submerged orifice above a gas chamber of finite volume. *Trans. Instn Chem. Engrs*, **47**, T241.

Lammers, J. H. and A. Biesheuvel, 1996. Concentration waves and the instability of bubbly flows. *J. Fluid Mech.*, **328**, 67.

LaNauze, R. D. and I. J. Harris, 1974. Gas bubble formation at elevated system pressures. *Trans. Instn Chem. Engrs.*, **52**, 337.

Letzel, H. M., J. C. Schouten, C. M. Van den Bleek, and R. Krishna, 1997. Influence of elevated pressure on the stability of bubbly flows. *Chem. Eng. Sci.*, **52**, 3733.

Letzel, M. H., J. C. Schouten, C. M. Van den Bleek, and R. Krishna, 1998. Effect of gas density on large-bubble holdup in bubble column reactors. *AIChE J.*, **44**, 2333.

Lee, D. J., X. Luo, and L.-S. Fan, 1998. Gas disengagement technique in a slurry bubble column operated in the coalesced bubble regime. *Chem. Eng. Sci.*, in press.

Levich, V. G., 1962. *Physiochemical Hydrodynamics*, Prentice Hall, Englewood Cliffs, NJ.

Li, H., and A. Prakash, 1997. Heat transfer and hydrodynamics in a three-phase slurry bubble column. *Ind. Eng. Chem. Res.*, **36**, 4688.

Lin, J. N., S. K. Banerji, and H. Yasuda, 1994. Role of interfacial tension in the formation and the detachment of air bubbles. 1. A single hold on a horizontal plane immersed in water. *Langmuir*, **10**, 936.

Lin, T.-J. and L.-S. Fan, 1997. Characteristics of high-pressure liquid-solid fluidization. *AIChE J.*, **43**, 45.

Lin, T.-J., K. Tsuchiya, and L.-S. Fan, 1998. Bubble flow characteristics in bubble columns at elevated pressure and temperature. *AIChE J.*, **44**, 545.

Lin, T.-J., G. B. Bass, K. Tsuchiya, and L.-S. Fan, 1999a. Distributor effects on hydrodynamics of high pressure bubble columns. *Chem. Eng. Sci.*, in review.

Lin, T.-J., K. Tsuchiya, and L.-S. Fan, 1999b. On the measurements of regime transition in high pressure bubble columns. *Can. J. Chem. Eng.*, in press.

Liu, T.-J. and S. G. Bankoff, 1993. Structure of air-water bubbly flow in a vertical pipe – II. Void fraction, bubble velocity, and bubble size distribution. *Int. J. Heat Mass Transfer*, **36**, 1061.

Luo, X., P. Jiang, and L.-S. Fan, 1997a. High pressure three-phase fluidization: hydrodynamics and heat transfer. *AIChE J.*, **43**, 2432.

Luo, X., J. Zhang, J., K. Tsuchiya, and L.-S. Fan, 1997b. On the rise velocity of bubbles in liquid-solid suspensions at elevated pressure and temperature. *Chem. Eng. Sci.*, **52**, 3693.

Luo, X., D. J. Lee, R. Lau, G. Q. Yang, and L.-S. Fan, 1998a. Maximum stable bubble size and gas holdup in high pressure slurry bubble columns. *AIChE J.*, in press.

Luo, X., K. Tsuchiya, and L.-S. Fan, 1998b. Gas jetting and bubble formation in high pressure liquid-solid suspensions. In *Fluidization IX*, edited by L.-S. Fan and T. M. Knowlton, Engineering Foundation, NY, 637.

Luo, X., G. Q. Yang, D. J. Lee, and L.-S. Fan, 1998c. Single bubble formation in high pressure liquid-solid suspensions. *Powder Technology*, **100**, 103.

Maneri, C. C., 1995. New look at wave analogy for prediction of bubble terminal velocities. *AIChE J.*, **41**, 481.

Massimilla, L., N. Majuri, and P. Signorini, 1959. Sull'assorbimento di gas in sistema: solido-liquido, fluidizzato. *La Ricerca Scientifica*, **29**, 1934.

Massimilla, L., A. Solimando, and E. Squillace, 1961. Gas dispersion in solid-liquid fluidized beds. *Brit. Chem. Eng.*, **6**, 232.

Mendelson, H. D., 1967. The motion of an air bubble rising in water. *AIChE J.*, **13**, 250.

Mill, P. L., J. R. Turner, P. A. Ramachandran, and M. P. Dudukovic, 1996. The Fischer-Tropsch synthesis in slurry bubble column reactors: Analysis of reactor performance using the axial dispersion model. *Three-phase sparged reactors*, Edited by K.D.P. Nigam and A. Schumpe, Gordon and Breach Publishers, 339.

Milne-Thomson, L. M., 1955. *Theoretical Hydrodynamics*, 3rd ed., Macmillan and Co., London.

Miyahara, T. K., K. Tsuchiya, and L.-S. Fan, 1989. Mechanism of particle entrainment in a gas-liquid-solid fluidized bed. *AIChE J.*, **35**, 1195.

O'Dowd, W., D. N. Smith, J. A. Ruether, and S. C. Saxena, 1987. Gas and solids behavior in a baffled and unbaffled slurry bubble column. *AIChE J.*, **33**, 1959.

Ostergaard, K., 1964. *Fluidization*, Soc. Chem. Ind., London.

Oyevaar, M. H., 1989. Gas-liquid contacting at elevated pressures. *Ph.D. thesis*, Twente Univ., The Netherlands.

Peng, X. D., B. A. Toseland, and P. J. A. Tijm, 1998. Kinetic understanding of chemical synergy in LPDME^{TM} process. Presented at *the 1998 AIChE Annual Meeting*, Nov. 15-20, Miami Beach, FL.

Petukhov, V. I. and V. A. Kolokol'tsev, 1965. Effect of liquid viscosity on droplet entrainment and volumetric air content. *Therm. Eng.*, **12**, 41.

Pinczewski, W. V., 1981. The formation and growth of bubbles at a submerged orifice. *Chem. Eng. Sci.*, **36**, 405.

Rados, N., 1999. Slurry bubble column hydrodynamics. D.Sc. proposal, Washington University, St. Louis.

Ramakrishnan, S., R. Kumar, and N. R. Kuloor, 1969. Studies in bubble formation – I: bubble formation under constant flow conditions. *Chem. Eng. Sci.*, **24**, 731.

Reid, R. C., J. M. Prausnitz, and T. K. Sherwood, 1977. *The Properties of Gases and Liquids*. McGraw-Hill, New York.

Reilly, I. G., D. S. Scott, T. J. W. de Bruijn, and D. MacIntyre, 1994. The role of gas phase momentum in determining gas holdup and hydrodynamic flow regimes in bubble column operations. *Can. J. Chem. Eng.*, **72**, 3.

Richardson, J. F., M. N. Roman, and K. J. Shakiri, 1976. Heat transfer from immersed surfaces in liquid fluidized beds. *Chem. Eng. Sci.*, **31**, 619.

Ruzicka, M. C., J. Drahos, J. Zahradnik, and N. H. Thomas, 1997. Intermittent transition from bubbling to jetting regime in gas-liquid two phase flows. *Int. J. Multiphase Flow*, **23**, 671.

Saberian-Broudjenni, M., G. Wild, J. C. Charpentier, Y. Fortin, J. P. Euzen, and R. Patoux, 1984. Contribution à l'ètude hydrodynamique des rèacteurs à lit fludisè gaz-liquide-solide, *Entropie*, No. 120, 30.

Sagert, N. H. and M. J. Quinn, 1977. Influence of high-pressure gases on the stability of thin aqueous films. *J. Colloid Int. Sci.*, **61**, 279.

Sagert, N. H. and M. J. Quinn, 1978. Surface viscosities at high pressure gas-liquid interfaces. *J. Colloid Int. Sci.*, **65**, 415.

Saxena, S. C., 1995. Bubble column reactors and Fischer-Tropsch synthesis. *Catal. Rev.-Sci. Eng.*, **37**, 227.

Saxena, S. C. and Z. D. Chen, 1994. Hydrodynamics and heat transfer of baffled and unbaffled slurry bubble columns. *Reviews in Chem. Eng.*, **10**, 193.

Saxena, S. C., N. S. Rao, and A. C. Saxena, 1990. Heat Transfer from a cylindrical probe immersed in a three-phase slurry bubble column. *Chem. Eng. J.*, **44**, 141.

Saxena, S. C., R. Vadivel, and A. C. Saxena, 1989. Gas holdup and heat transfer from immersed surfaces in two- and three-phase systems in bubble columns. *Chem. Eng. Comm.*, **85**, 63.

Schumpe, A. and G. Grund, 1986. The gas disengagement technique for studying gas holdup structure in bubble columns. *Can. J. Chem. Eng.*, **64**, 891.

Shnip, A. I., R. V. Kolhatkar, D. Swamy, and J. B. Joshi, 1992. Criteria for the transition from the homogeneous to the heterogeneous regime in two-dimensional bubble column reactors. *Int. J. Multiphase Flow*, **18**, 705.

Shah, Y. T., B. G. Kelkar, S. P. Godbole, and W.-D. Deckwer, 1982. Design parameters estimations for bubble column reactors. *AIChE J.*, **28**, 353.

Shollenberger, K. A. and T. J. O'Hern, 1997. Characterization of slurry-phase flow in the Laporte alternative fuels development unit (AFDU) using differential pressure measurements. *U.S. DOE Report*, DE-FC22-95 PC 95051.

Soong, Y., F. W. Harke, I. K. Gamwo, R. R. Schehl, and M. F. Zarochak, 1997. Hydrodynamic study in a slurry-bubble-column reactor. *Catalysis Today*, **35**, 427.

Sriram, K. and R. Mann, 1977. Dynamic gas disengagement: A new technique for assessing the behaviour of bubble columns. *Chem. Eng. Sci.*, **32**, 571.

Tarmy, B., M. Chang, C. Coulaloglou, and P. Ponzi, 1984. Hydrodynamic characteristics of three phase reactors. *The Chemical Engineer*, Oct., No. 407, 18.

Tomiyama, A., I. Kataoka, and T. Sakaguchi, 1995. Drag coefficients of bubbles (1st report, drag coefficients of a single bubble in a stagnant liquid). *Nippon Kikai Gakkai Ronbunshu B Hen*, **61**(587), 2357.

Tsuchiya, K., A. Furumoto, L.-S. Fan, and J. Zhang, 1997. Suspension viscosity and bubble velocity in liquid-solid fluidized beds. *Chem. Eng. Sci.*, **52**, 3053.

Tsuchiya, K. and O. Nakanishi, 1992. Gas holdup behavior in a tall bubble column with perforated plate distributors. *Chem. Eng. Sci.*, **47**, 3347.

Tsuchiya, K., G.-H. Song, W.-T. Tang, and L.-S. Fan, 1992. Particle drift induced by a bubble in a liquid-solid fluidized bed with low-density particles, *AIChE J.*, **38**, 1847.

Tsuge, H., Y. Nakajima, and K. Terasaka, 1992. Behavior of bubbles formed from a submerged orifice under high system pressure. *Chem. Eng. Sci.*, **47**, 3273.

Vrij, A., 1966. Possible mechanism for the spontaneous rupture of thin, free liquid films. *Disc. Faraday Soc.*, **42**, 23.

Wallis, G. B., 1969. *One-Dimensional Two-Phase Flow*, McGraw-Hill, New York.

Walter, J. F. and H. W. Blanch, 1986. Bubble break-Up in gas-liquid bioreactors: break-up in turbulent flows. *Chem. Eng. J.*, **32**, B7.

Wasan, D. T. and M. S. Ahluwalia, 1969. Consecutive film and surface renewal mechanism for heat and mass transfer from a wall. *Chem. Eng. Sci.*, **24**, 1535.

Wilkinson, P. M., A. P. Sper, and L. L. Van Dierendonck, 1992. Design parameters estimation for scale-up of high-pressure bubble columns. *AIChE J.*, **38**, 544.

Wilkinson, P. M. and L. L. Van Dierendonck, 1990. Pressure and gas density effects on bubble break-up and gas hold-up in bubble columns. *Chem. Eng. Sci.*, **45**, 2309.

Wilkinson, P. M. and L. L. Van Dierendonck , 1994. A theoretical model for the influence of gas properties and pressure on single-bubble formation at an orifice. *Chem. Eng. Sci.*, **49**, 1429.

Yang, G. Q., X. Luo, R. Lau, and L.-S. Fan, 1998. Heat transfer characteristics in a high pressure slurry bubble column. Presented at *the 1998 AIChE Annual Meeting*, paper 191b, Nov. 15-20, Miami Beach, FL.

Yang, G. Q., X. Luo, R. Lau, and L.-S. Fan, 1999. Single bubble formation in high pressure liquid-solid suspensions with pressure fluctuations in the gas chamber. *Chem. Eng. Sci.*, in review.

Yoo, D.-H., H. Tsuge, K. Terasaka, and K. Mizutani, 1997. Behavior of bubble formation in suspended solution for an elevated pressure system. *Chem. Eng. Sci.*, **52**, 3701.

Yu, Y. H. and S. D. Kim, 1991. Bubble properties and local liquid velocity in the radial direction of cocurrent gas-liquid flow. *Chem. Eng. Sci.*, **46**, 313.

Zahradnik, J., M. Fialova, M. Ruzicka, J. Drahos, F. Kastanek, and N. H. Thomas, 1997. Duality of the gas-liquid flow regimes in bubble column reactors, *Chem. Eng. Sci.*, **52**, 3811.

Zhang, J., L.-S. Fan, C. Zhu, R. Pfeffer, and D. Qi, 1998a. Dynamic behavior of collinear collision of elastic spheres in viscous fluids, *Advanced Technologies for Particle Processing*, Vol. II, 44, Particle Technology Forum, AIChE; *Proceedings* of *PTF*

Topical Conference at AIChE Annual Meeting, Nov. 15-20, Miami Beach, FL; *Powder Technology*, in press.

Zhang, J., Y. Li, and L.-S. Fan, 1998b. Numerical simulation of gas-liquid-solid fluidization systems using a combined CFD-DPM-VOF method: single bubble rise behavior, *Advanced Technologies for Particle Processing*, Vol. II, 509, Particle Technology Forum, AIChE; *Proceedings* of *PTF Topical Conference at AIChE Annual Meeting*, Nov. 15-20, Miami Beach, FL.

FIGURES

Figure 1 Effect of pressure on terminal rise velocity of single bubbles and predicted values at (a) 27°C and (b) 78°C.

Figure 2 Comparisons of measured and calculated *Re* of single bubbles in Paratherm NF heat transfer fluid under varied pressure and temperature conditions. The Fan-Tsuchiya (1990) and Tomiyama *et al.* (1995) correlations are plotted (—— and — – —, respectively) at regular intervals of *Mo* values. The Fan-Tsuchiya correlation at measured *Mo* values for comparison with measured *Re-Eo* data (—).

Figure 3 Effect of pressure on bubble rise velocity in a fluidized bed at (a) 26.5°C and (b) 87.5°C. Solids holdups for +, open, and filled symbols are 0, 0.384, and 0.545, respectively.

Figure 4 Effect of pressure on bubble rise velocity in a fluidized bed at (a) 26.5°C and (b) 87.5°C. Solids holdups for +, open, and filled symbols are 0, 0.381, and 0.555, respectively.

Figure 5 Simulation and experimental results of a bubble rising in a liquid-solid fluidized bed.

Figure 6 Simulation of a bubble emerging from a liquid-solid fluidized bed.

Figure 7 Simulation results of a single bubble rising at $P = 19.4$ MPa.

Figure 8 The balance of all the forces acting on a growing bubble.

Figure 9 Comparison between the experimental data and model predictions of initial bubble size in high-pressure liquid-solid suspensions. Lines and symbols represent the model predictions and experimental data, respectively.

Figure 10 Initial bubble size in liquid-solid suspensions as a function of pressure and gas velocity for bubble formation with pressure fluctuation in the gas chamber.

Figure 11 A series of photographs showing the bubbling-jetting transition at $P = 4.24$ MPa and $T = 28$°C for (a) $u_o = 0.27$ m/s and $Re_o = 1{,}075$; (b) $u_o = 1.35$ m/s and $Re_o = 5{,}321$; (c) $u_o = 2.23$ m/s and $Re_o = 8{,}809$; (d) $u_o = 2.60$ m/s and $Re_o = 10{,}243$; (e) $u_o = 3.99$ m/s and $Re_o = 15{,}759$; (f) $u_o = 6.42$ m/s and $Re_o = 25{,}355$.

Figure 12 Schematic of the internal circulation model for bubble breakup.

Figure 13 A sequence of bubble images showing the process of bubble breakup at $P = 3.5$ MPa.

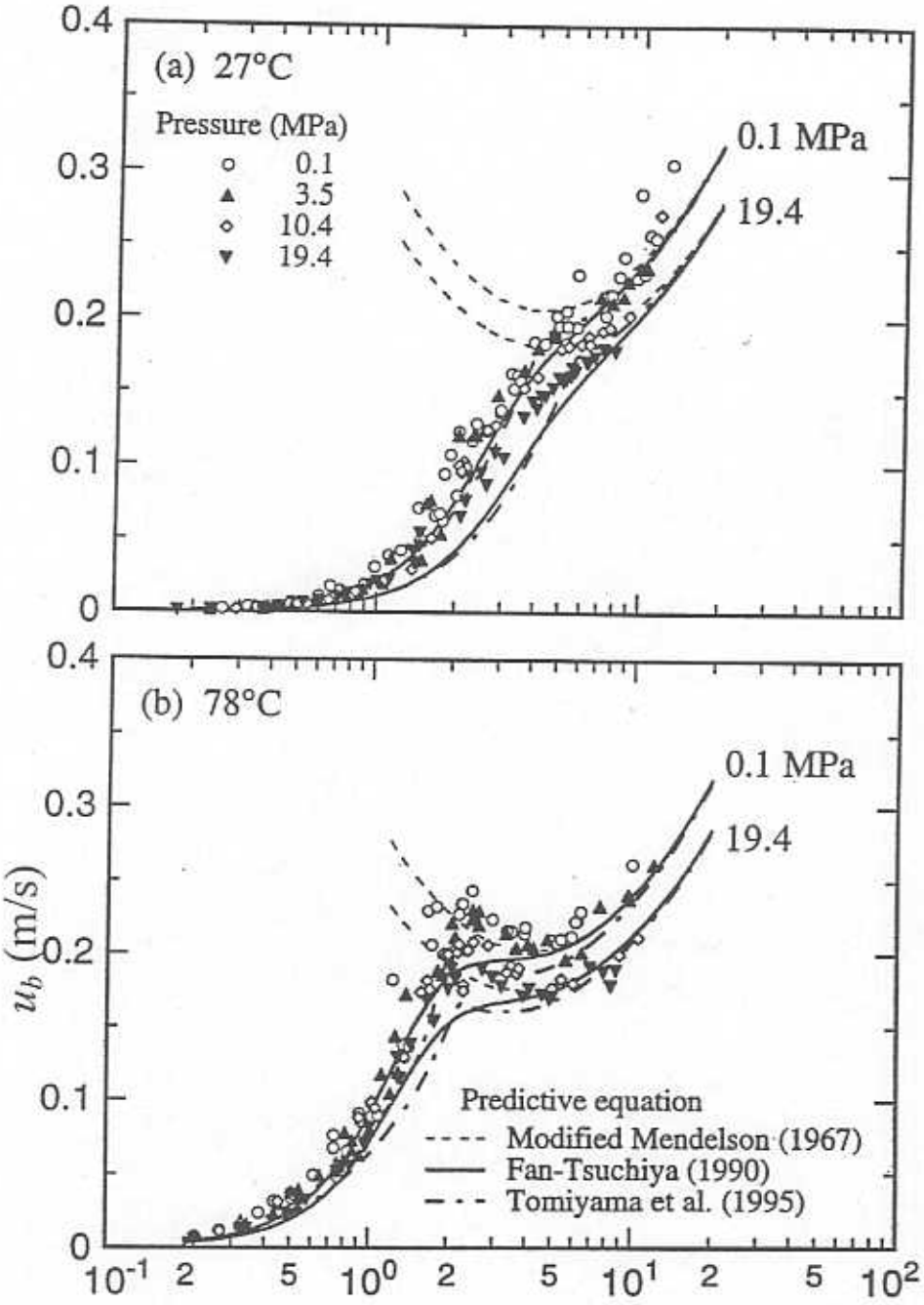
(a) 27°C
Pressure (MPa)
0.1
3.5
10.4
19.4
0.1 MPa
19.4
(b) 78°C
0.1 MPa
19.4
u_b (m/s)
Predictive equation
Modified Mendelson (1967)
Fan-Tsuchiya (1990)
Tomiyama et al. (1995)
0.4
0.3
0.2
0.1
0
10^{-1} 2 5 10^{0} 2 5 10^{1} 2 5 10^{2}

Figure 1

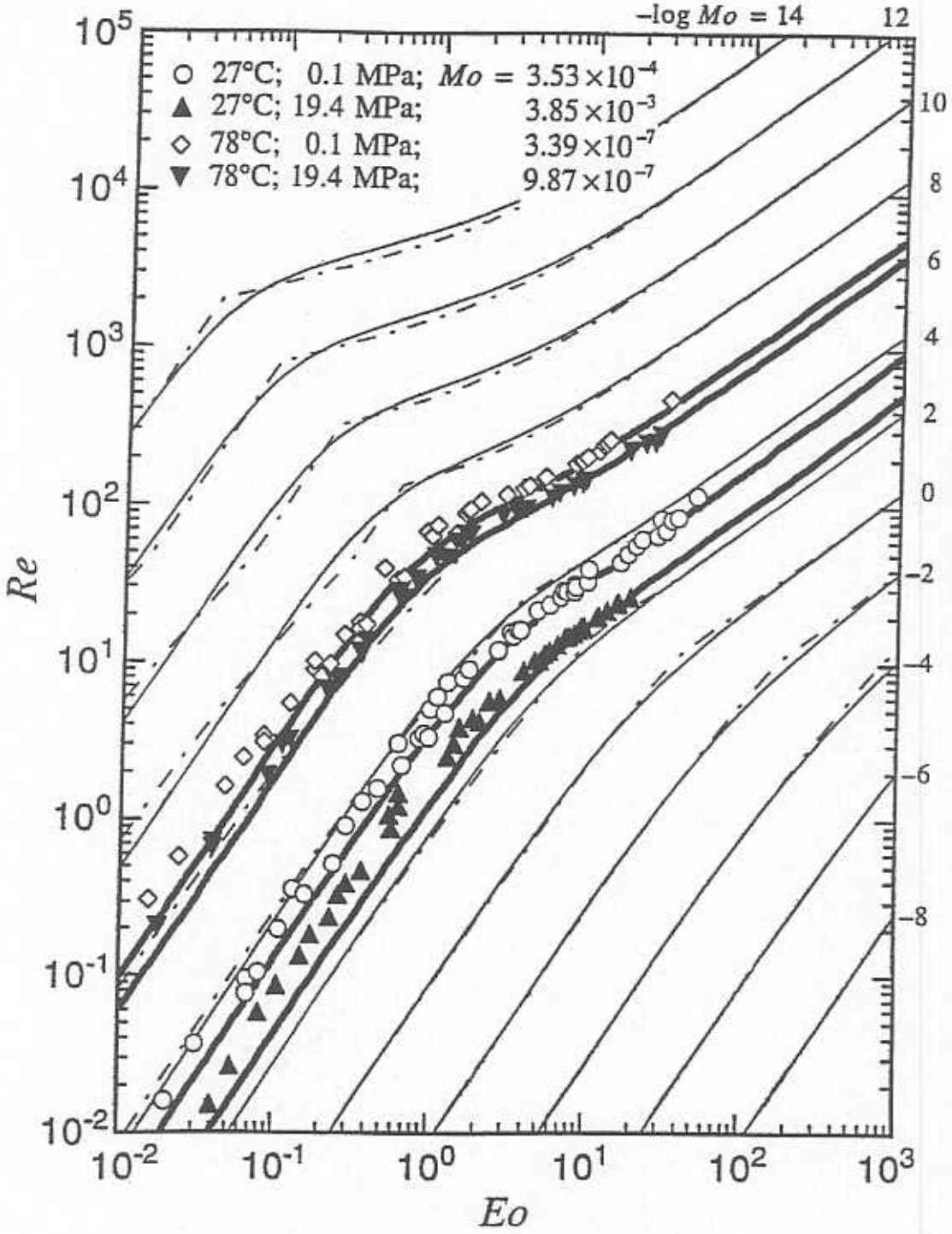
−log Mo = 14
12
10
8
6
4
2
0
−2
−4
−6
−8
○ 27°C; 0.1 MPa; Mo = 3.53×10⁻⁴
▲ 27°C; 19.4 MPa; 3.85×10⁻³
◇ 78°C; 0.1 MPa; 3.39×10⁻⁷
▼ 78°C; 19.4 MPa; 9.87×10⁻⁷
10⁵
10⁴
10³
10²
10¹
10⁰
10⁻¹
10⁻²
Re
10⁻²
10⁻¹
10⁰
10¹
10²
10³
Eo

Figure 2

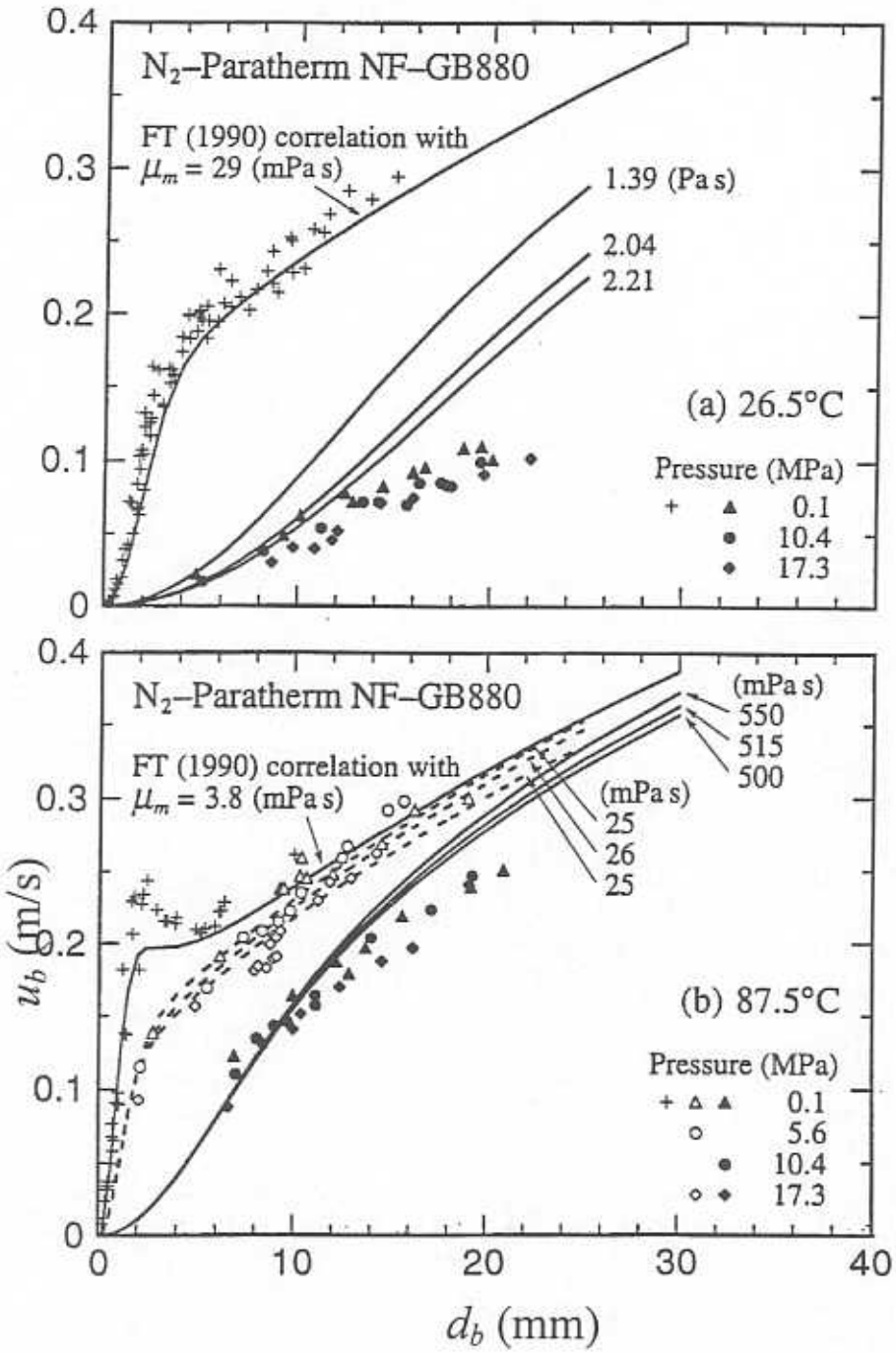
N2–Paratherm NF–GB880
FT (1990) correlation with
μm = 29 (mPa s)
1.39 (Pa s)
2.04
2.21
(a) 26.5°C
Pressure (MPa)
0.1
10.4
17.3
N2–Paratherm NF–GB880
FT (1990) correlation with
μm = 3.8 (mPa s)
(mPa s)
550
515
500
(mPa s)
25
26
25
(b) 87.5°C
Pressure (MPa)
0.1
5.6
10.4
17.3
ub (m/s)
db (mm)
0
0.1
0.2
0.3
0.4
10
20
30
40

Figure 3

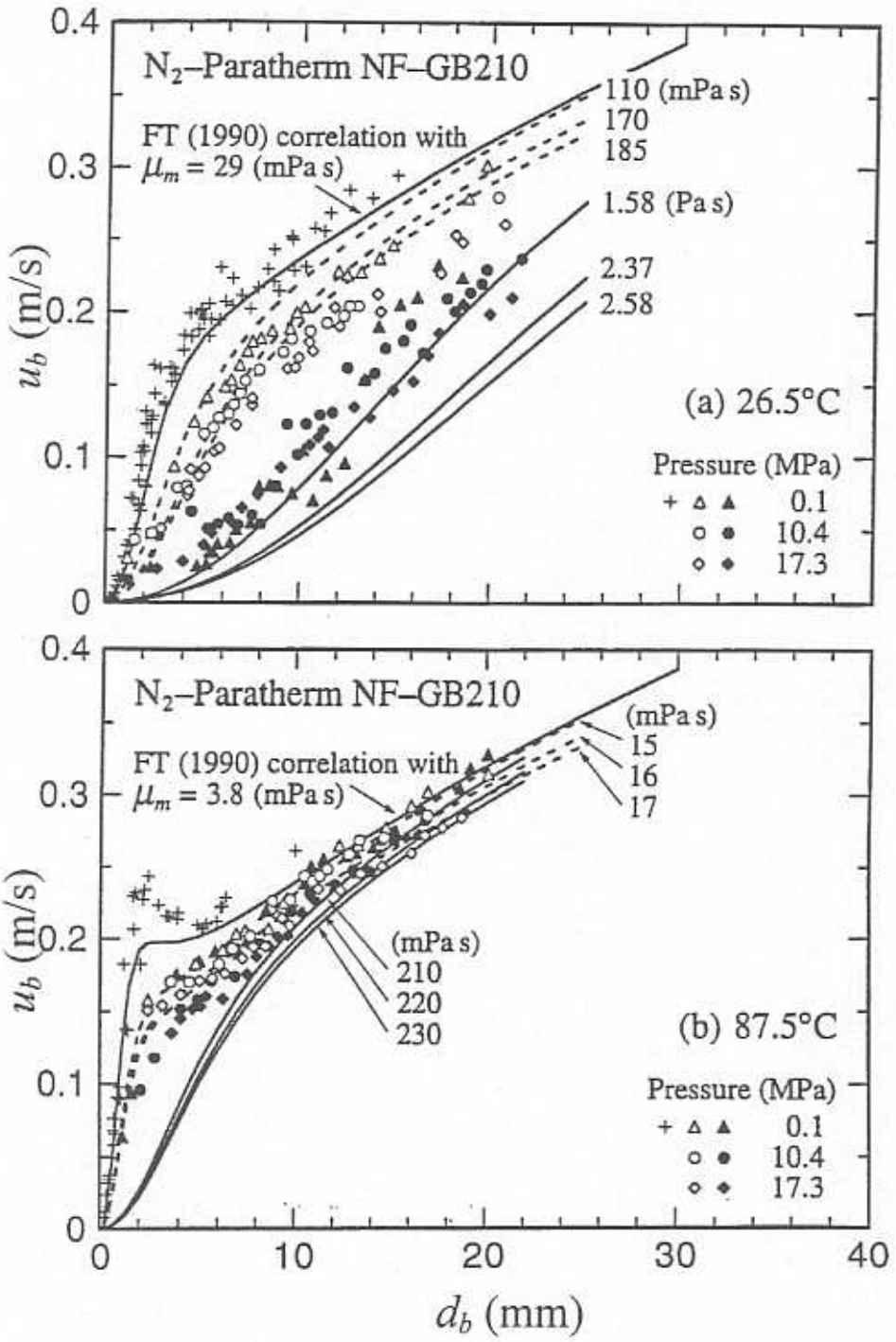
N2–Paratherm NF–GB210
FT (1990) correlation with
μm = 29 (mPa s)
110 (mPa s)
170
185
1.58 (Pa s)
2.37
2.58
(a) 26.5°C
Pressure (MPa)
0.1
10.4
17.3
N2–Paratherm NF–GB210
FT (1990) correlation with
μm = 3.8 (mPa s)
(mPa s)
15
16
17
(mPa s)
210
220
230
(b) 87.5°C
Pressure (MPa)
0.1
10.4
17.3
ub (m/s)
db (mm)
0
0.1
0.2
0.3
0.4
10
20
30
40

Figure 4

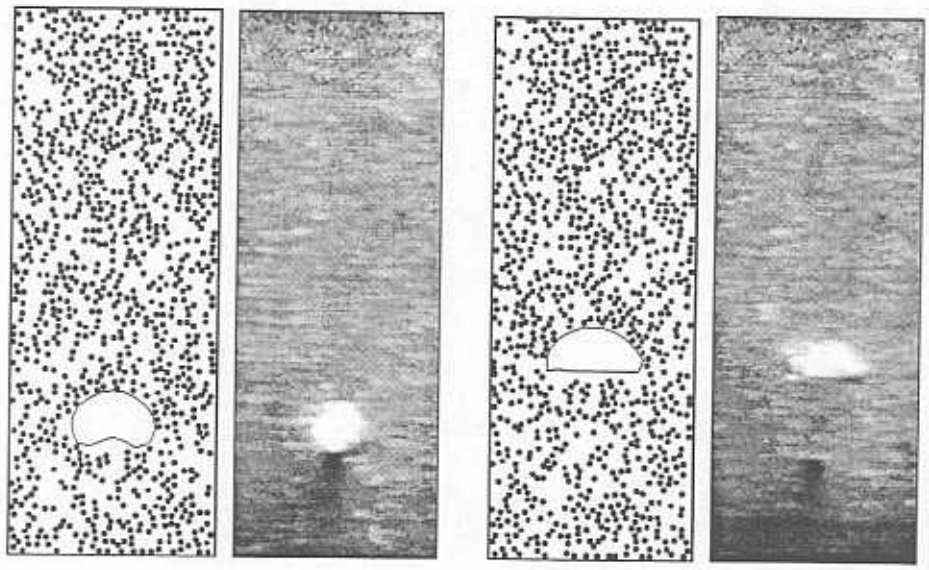

(a) $t = 0.06$ s (b) $t = 0.16$ s

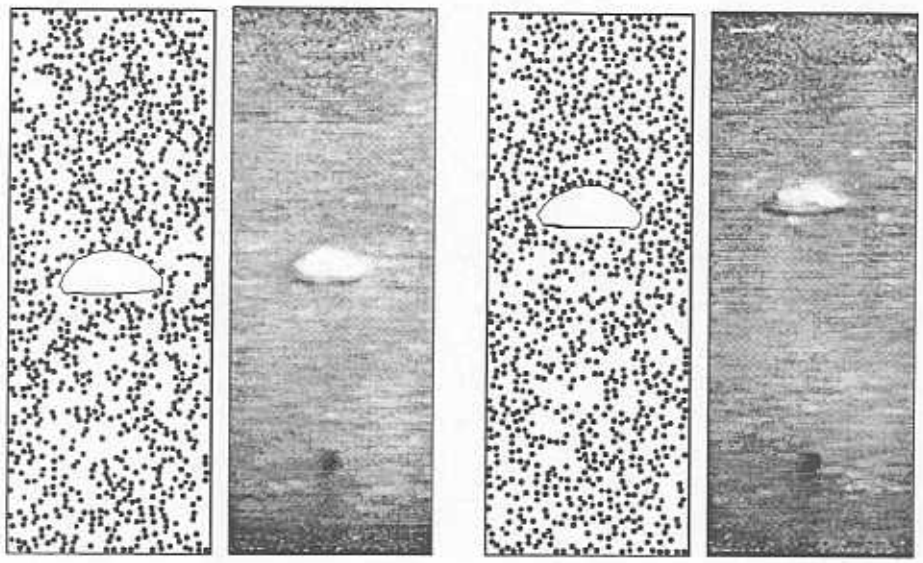

(c) $t = 0.26$ s (d) $t = 0.36$ s

Figure 5

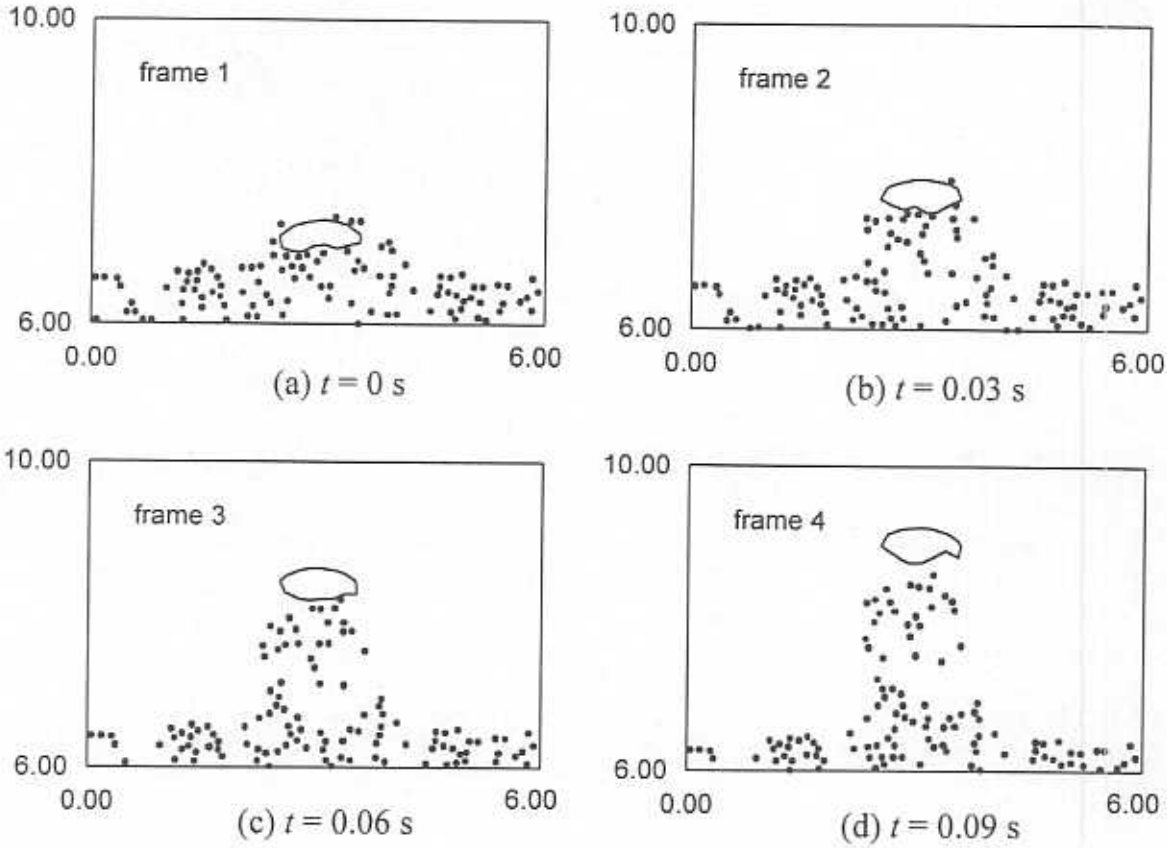
10.00
frame 1
6.00
0.00
6.00
(a) $t = 0$ s
10.00
frame 2
6.00
0.00
6.00
(b) $t = 0.03$ s
10.00
frame 3
6.00
0.00
6.00
(c) $t = 0.06$ s
10.00
frame 4
6.00
0.00
6.00
(d) $t = 0.09$ s

Figure 6

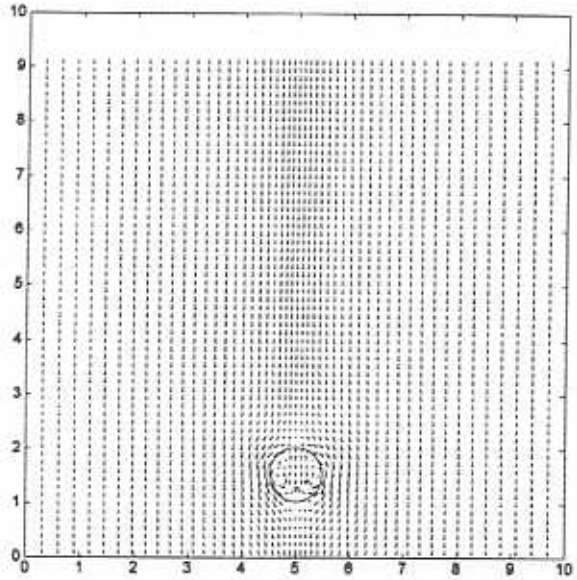

(a) $t = 0$ s

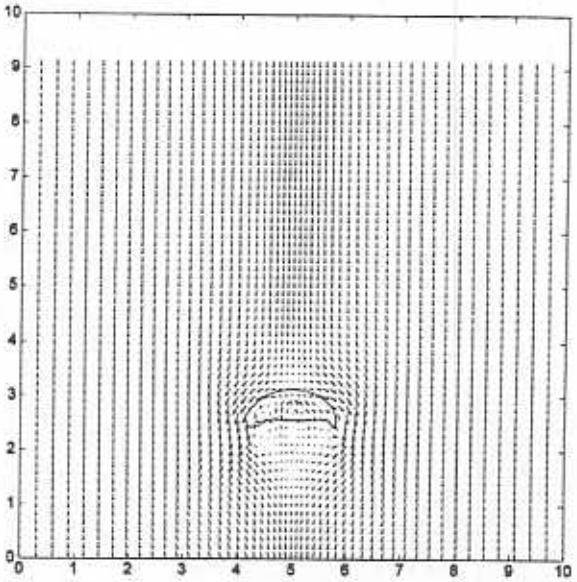

(b) $t = 0.06$ s

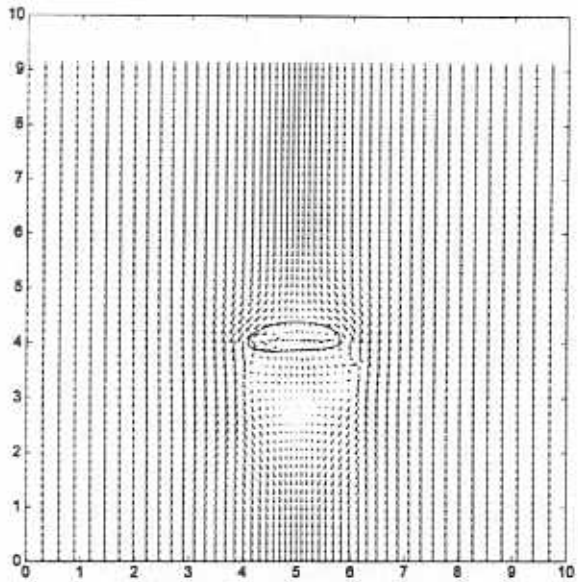

(c) $t = 0.12$ s

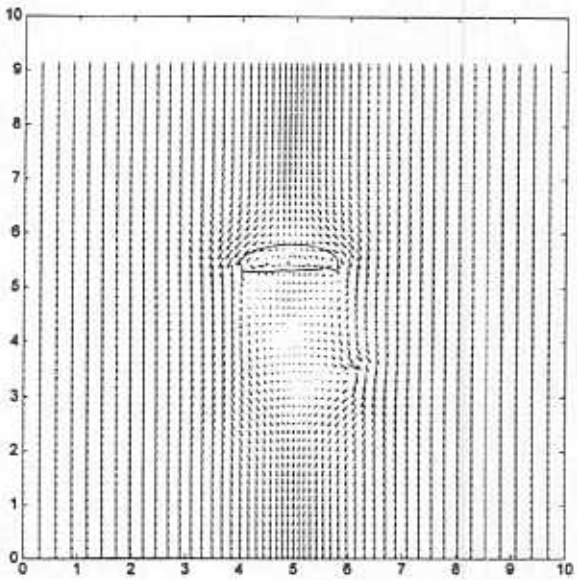

(d) $t = 0.18$ s

Figure 7

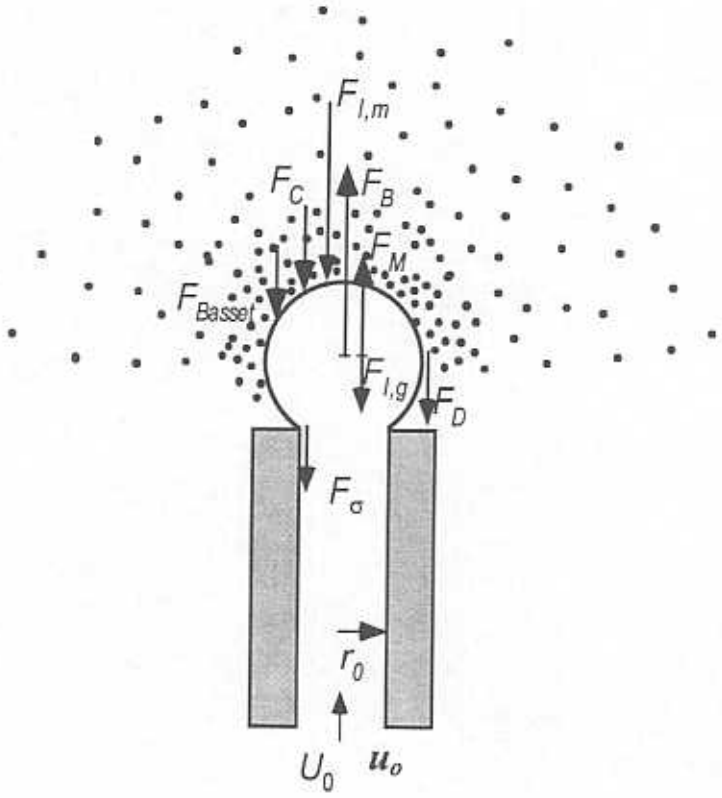

Figure 8

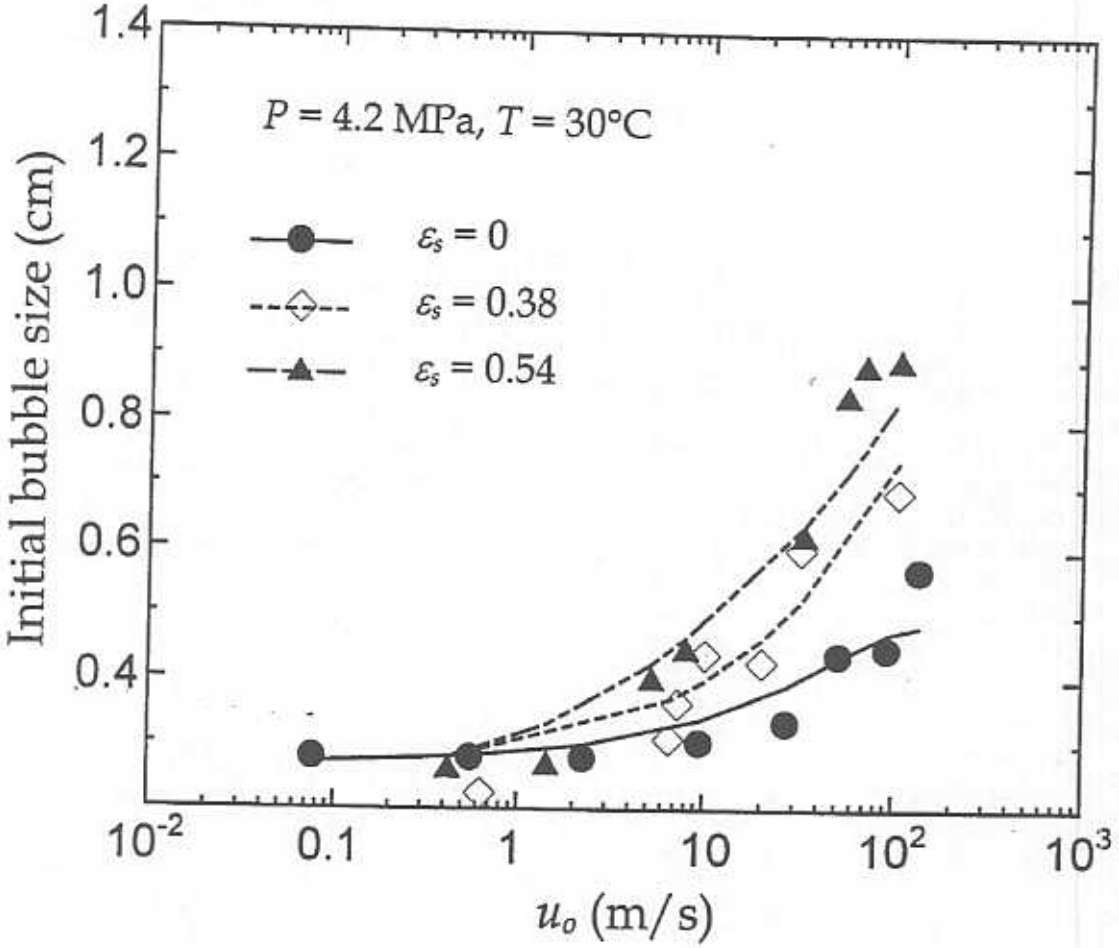
1.4
1.2
1.0
0.8
0.6
0.4
Initial bubble size (cm)
P = 4.2 MPa, T = 30°C
εs = 0
εs = 0.38
εs = 0.54
10-2
0.1
1
10
10²
10³
uo (m/s)

Figure 9

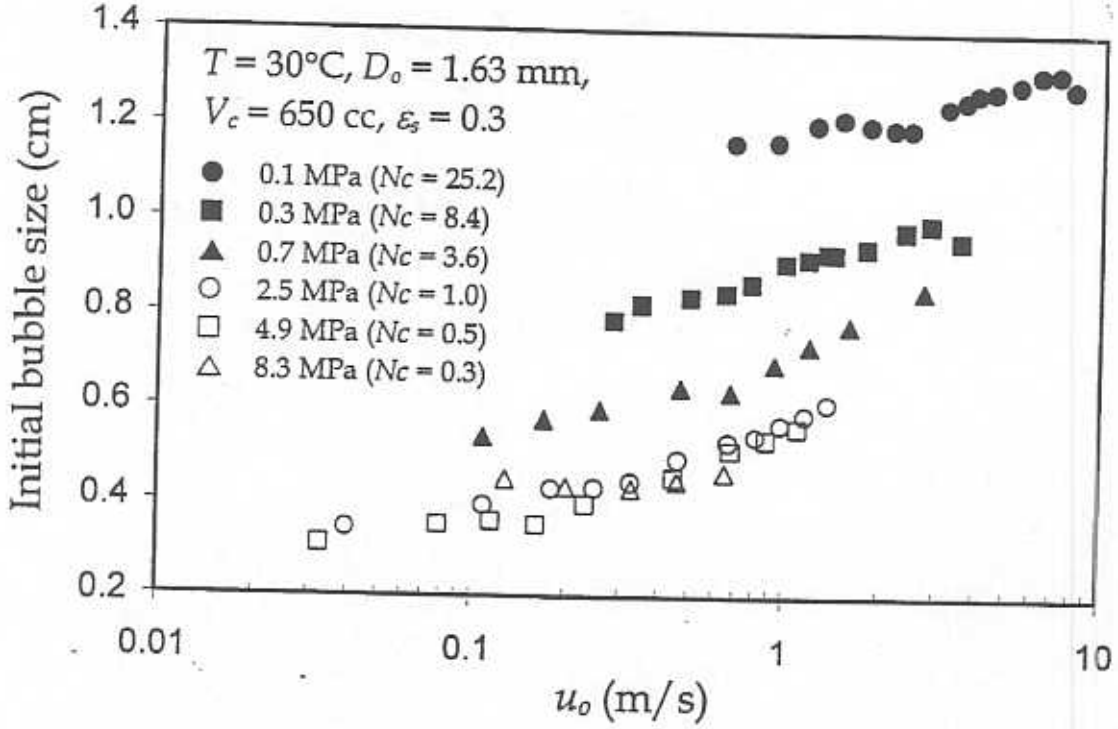
T = 30°C, D_o = 1.63 mm,
V_c = 650 cc, ε_s = 0.3
0.1 MPa (Nc = 25.2)
0.3 MPa (Nc = 8.4)
0.7 MPa (Nc = 3.6)
2.5 MPa (Nc = 1.0)
4.9 MPa (Nc = 0.5)
8.3 MPa (Nc = 0.3)
Initial bubble size (cm)
1.4
1.2
1.0
0.8
0.6
0.4
0.2
0.01
0.1
1
10
u_o (m/s)

Figure 10

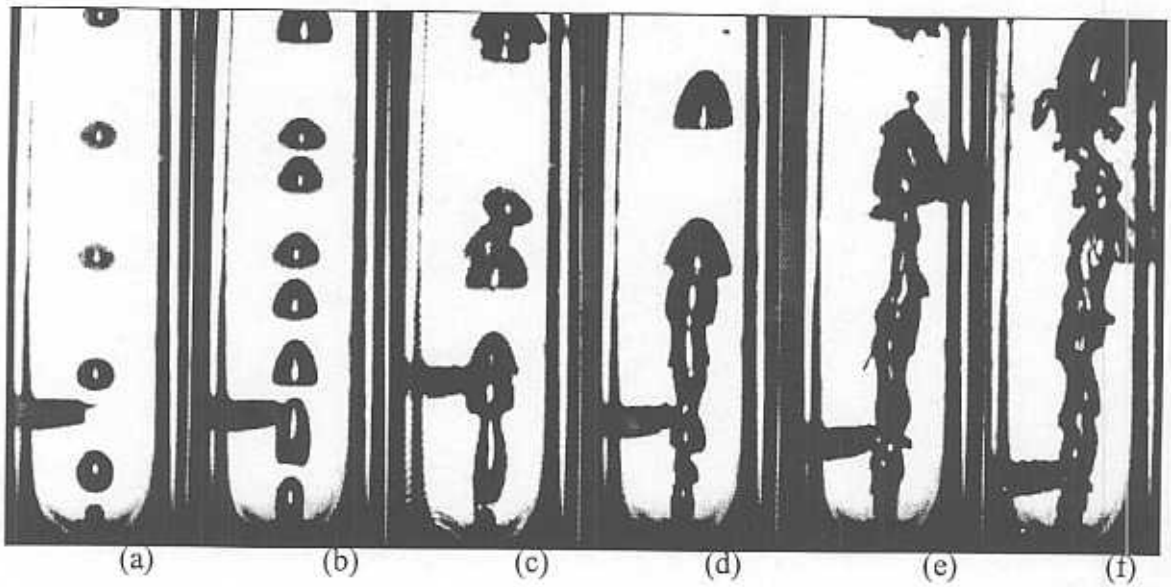

Figure 11

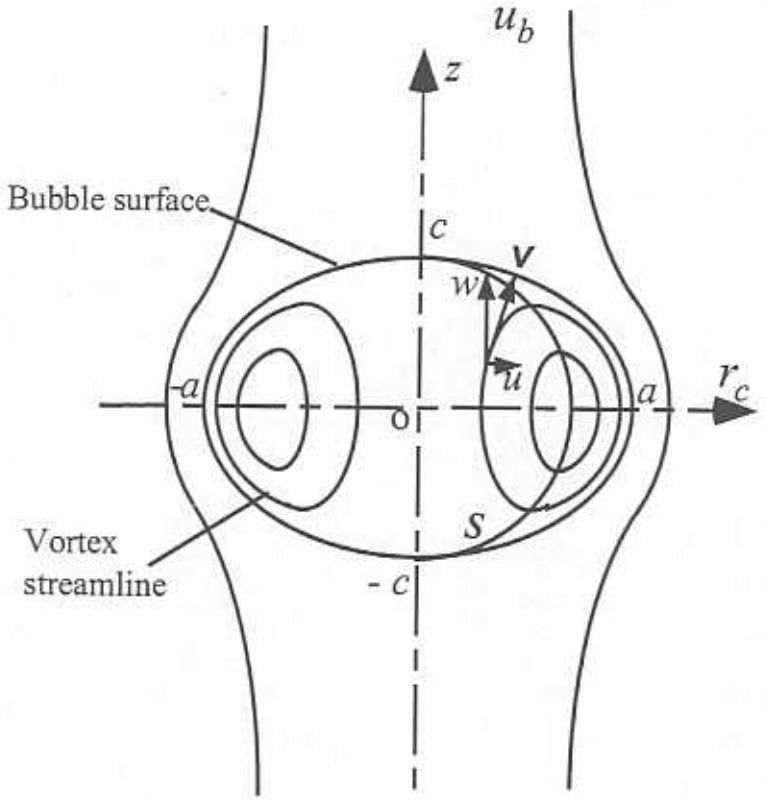

Figure 12

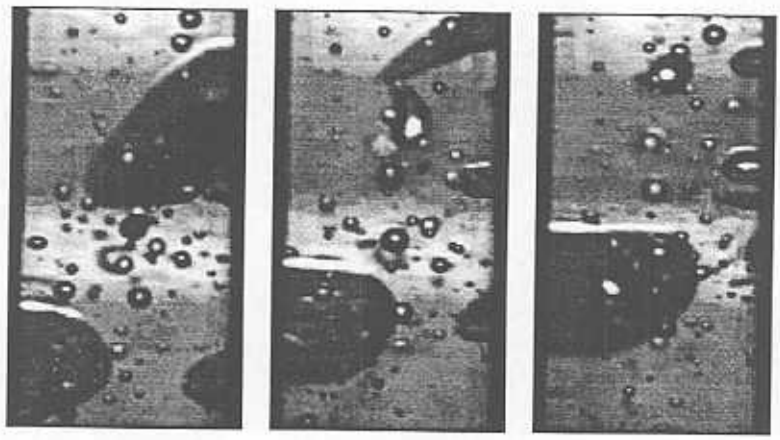

(a) $t = 0$ (b) $t = 0.017$ s (c) $t = 0.034$ s

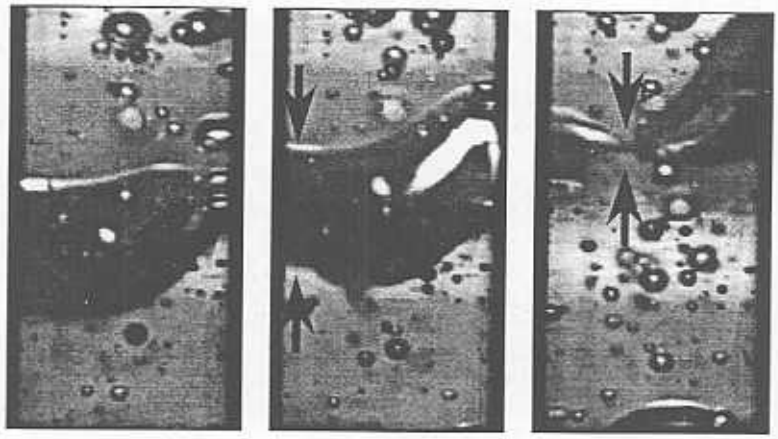

(d) $t = 0.052$ s (e) $t = 0.068$ s (f) $t = 0.085$ s

Figure 13

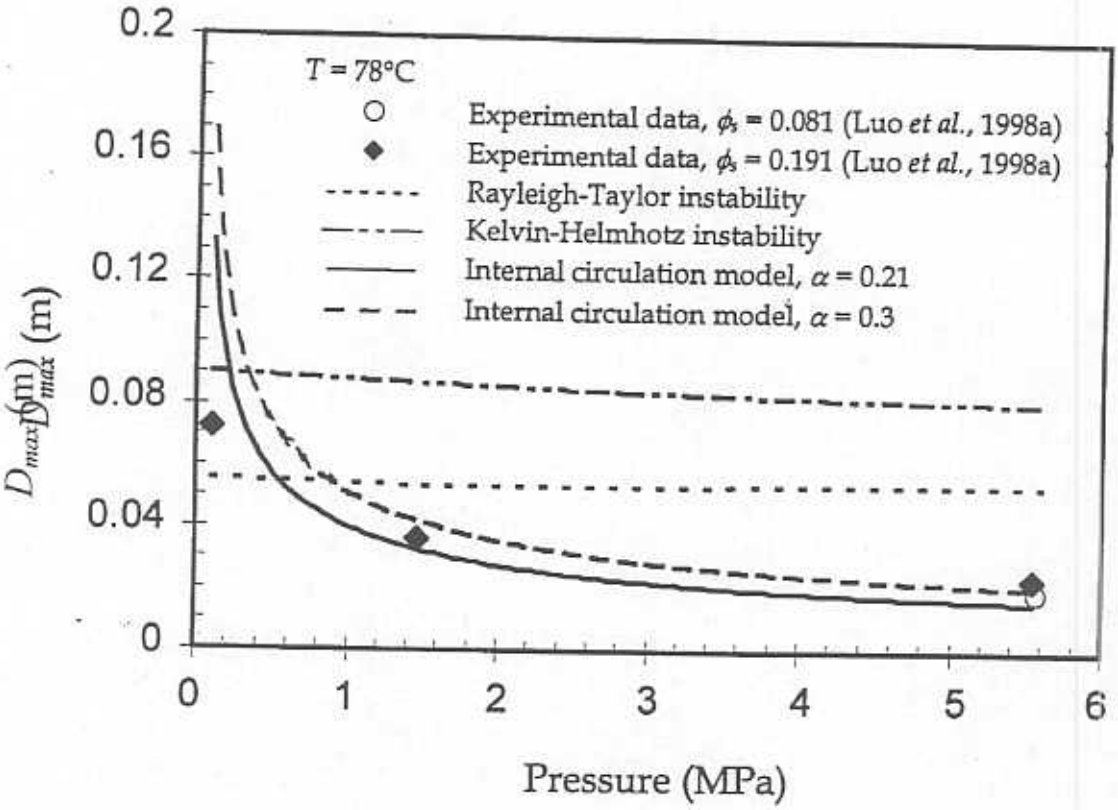
T = 78°C
Experimental data, ϕ_s = 0.081 (Luo et al., 1998a)
Experimental data, ϕ_s = 0.191 (Luo et al., 1998a)
Rayleigh-Taylor instability
Kelvin-Helmhotz instability
Internal circulation model, α = 0.21
Internal circulation model, α = 0.3
D_{max} (m)
0.2
0.16
0.12
0.08
0.04
0
0
1
2
3
4
5
6
Pressure (MPa)

Figure 14(a)

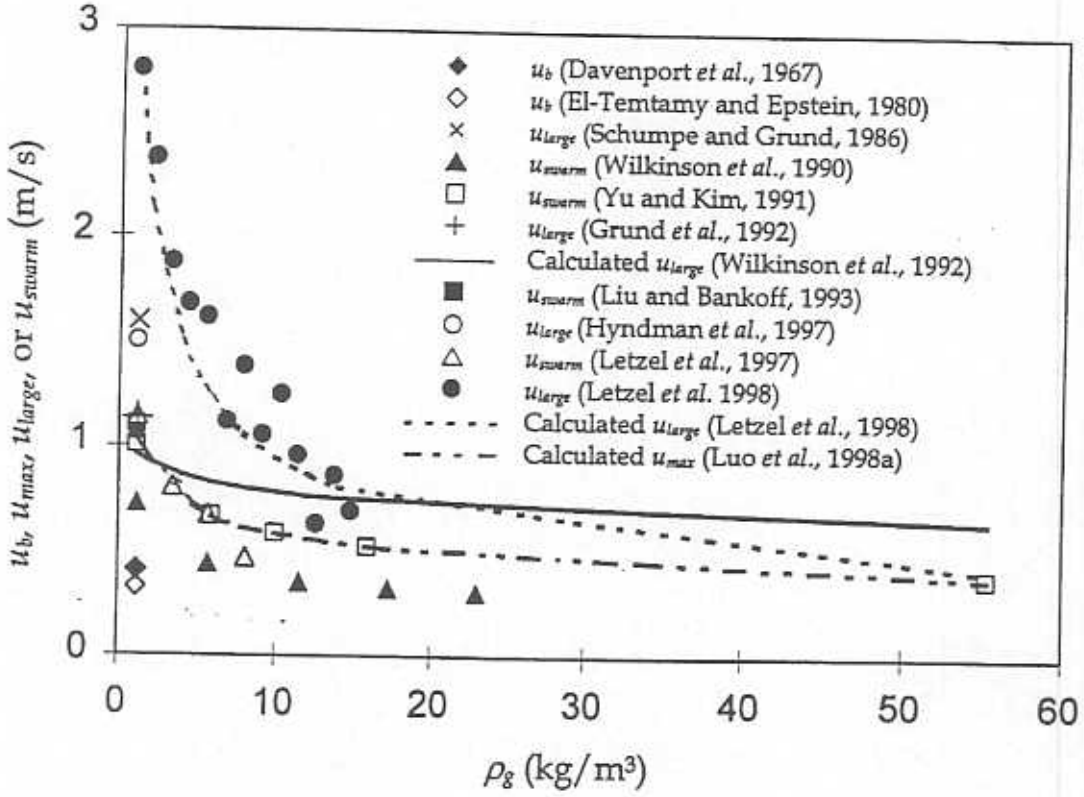
3
2
1
0
0
10
20
30
40
50
60
u_b, u_{max}, u_{large}, or u_{swarm} (m/s)
ρ_g (kg/m³)
u_b (Davenport *et al.*, 1967)
u_b (El-Temtamy and Epstein, 1980)
u_{large} (Schumpe and Grund, 1986)
u_{swarm} (Wilkinson *et al.*, 1990)
u_{swarm} (Yu and Kim, 1991)
u_{large} (Grund *et al.*, 1992)
Calculated u_{large} (Wilkinson *et al.*, 1992)
u_{swarm} (Liu and Bankoff, 1993)
u_{large} (Hyndman *et al.*, 1997)
u_{swarm} (Letzel *et al.*, 1997)
u_{large} (Letzel *et al.* 1998)
Calculated u_{large} (Letzel *et al.*, 1998)
Calculated u_{max} (Luo *et al.*, 1998a)

Figure 14(b)

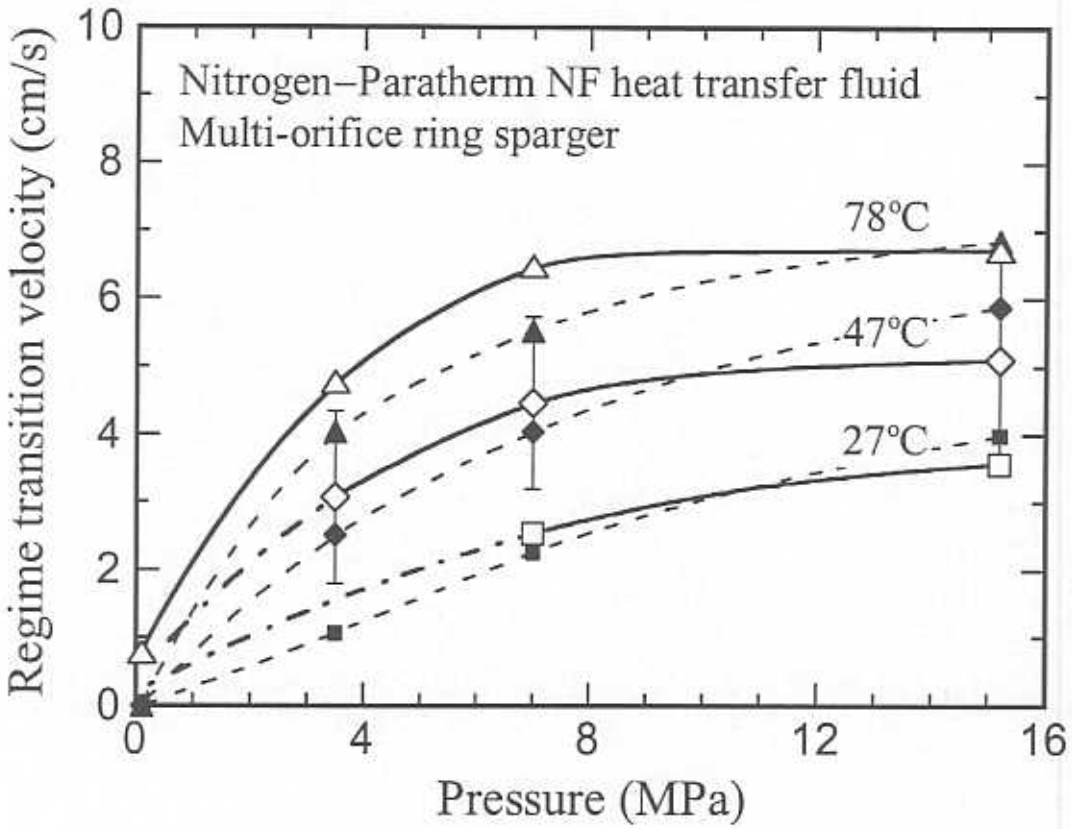
Nitrogen–Paratherm NF heat transfer fluid
Multi-orifice ring sparger
78°C
47°C
27°C
Regime transition velocity (cm/s)
Pressure (MPa)
0
2
4
6
8
10
0
4
8
12
16

Figure 15(a)

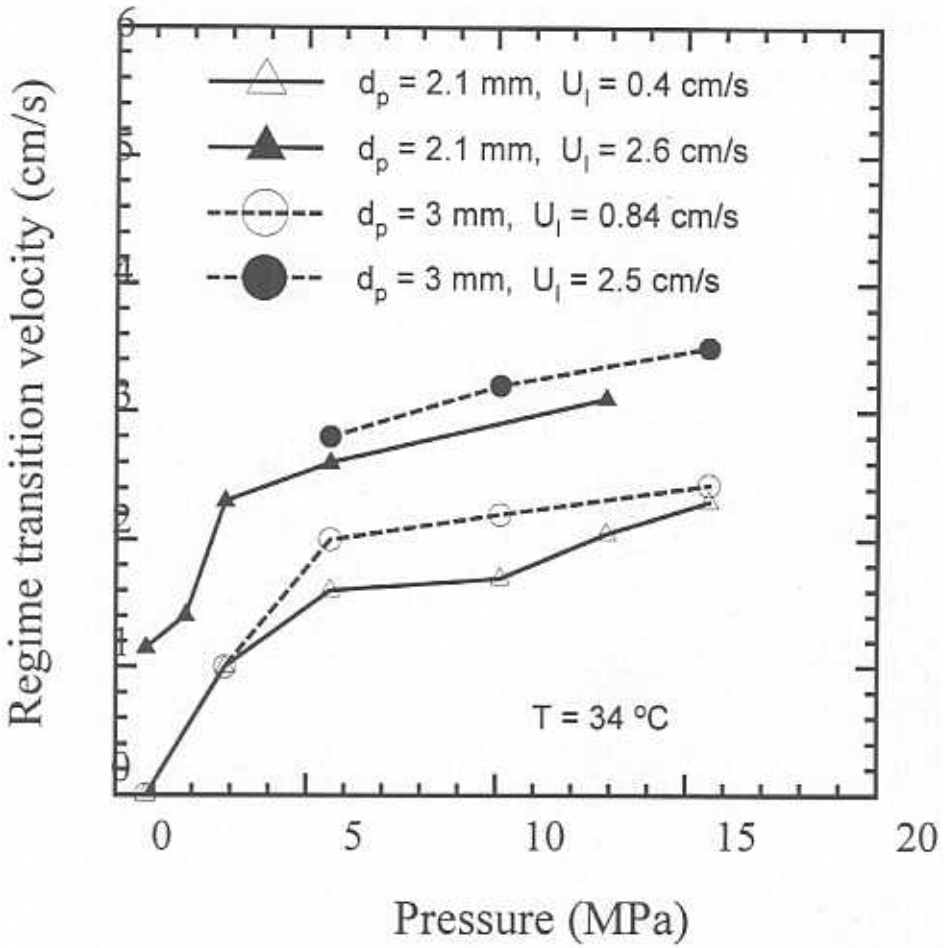
Regime transition velocity (cm/s)
d_p = 2.1 mm, U_l = 0.4 cm/s
d_p = 2.1 mm, U_l = 2.6 cm/s
d_p = 3 mm, U_l = 0.84 cm/s
d_p = 3 mm, U_l = 2.5 cm/s
T = 34 °C
0
5
10
15
20
Pressure (MPa)

Figure 15(b)

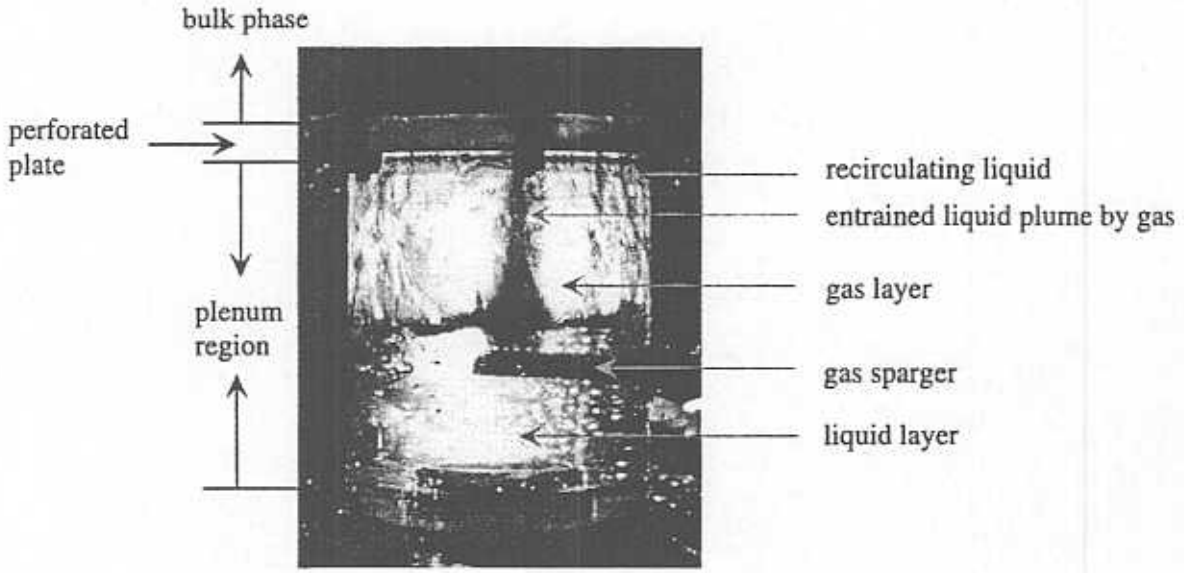
bulk phase
perforated plate
plenum region
recirculating liquid
entrained liquid plume by gas
gas layer
gas sparger
liquid layer

Figure 16

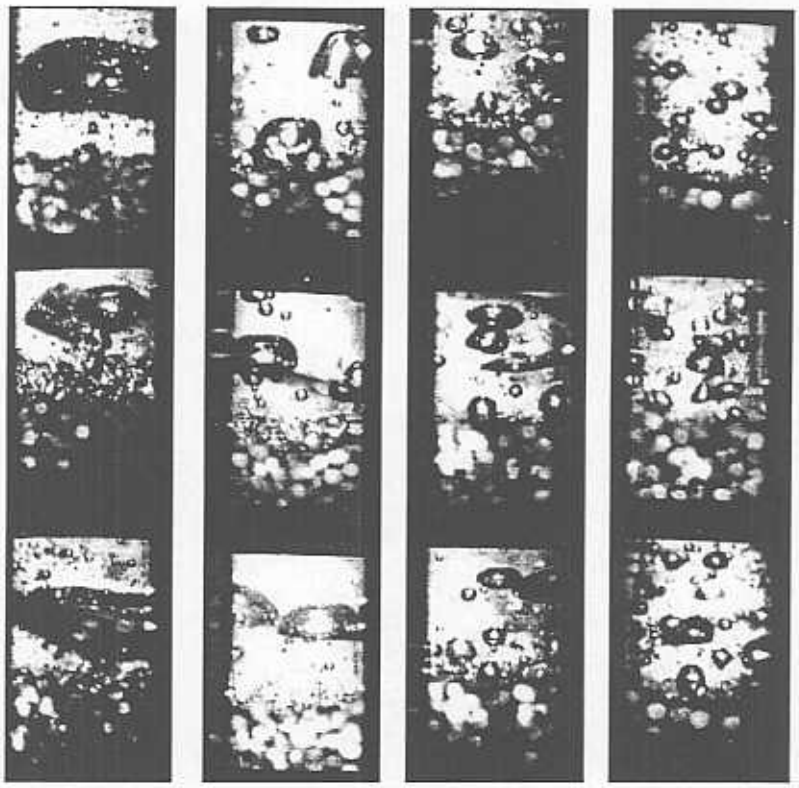

(a) (b) (c) (d)

Figure 17

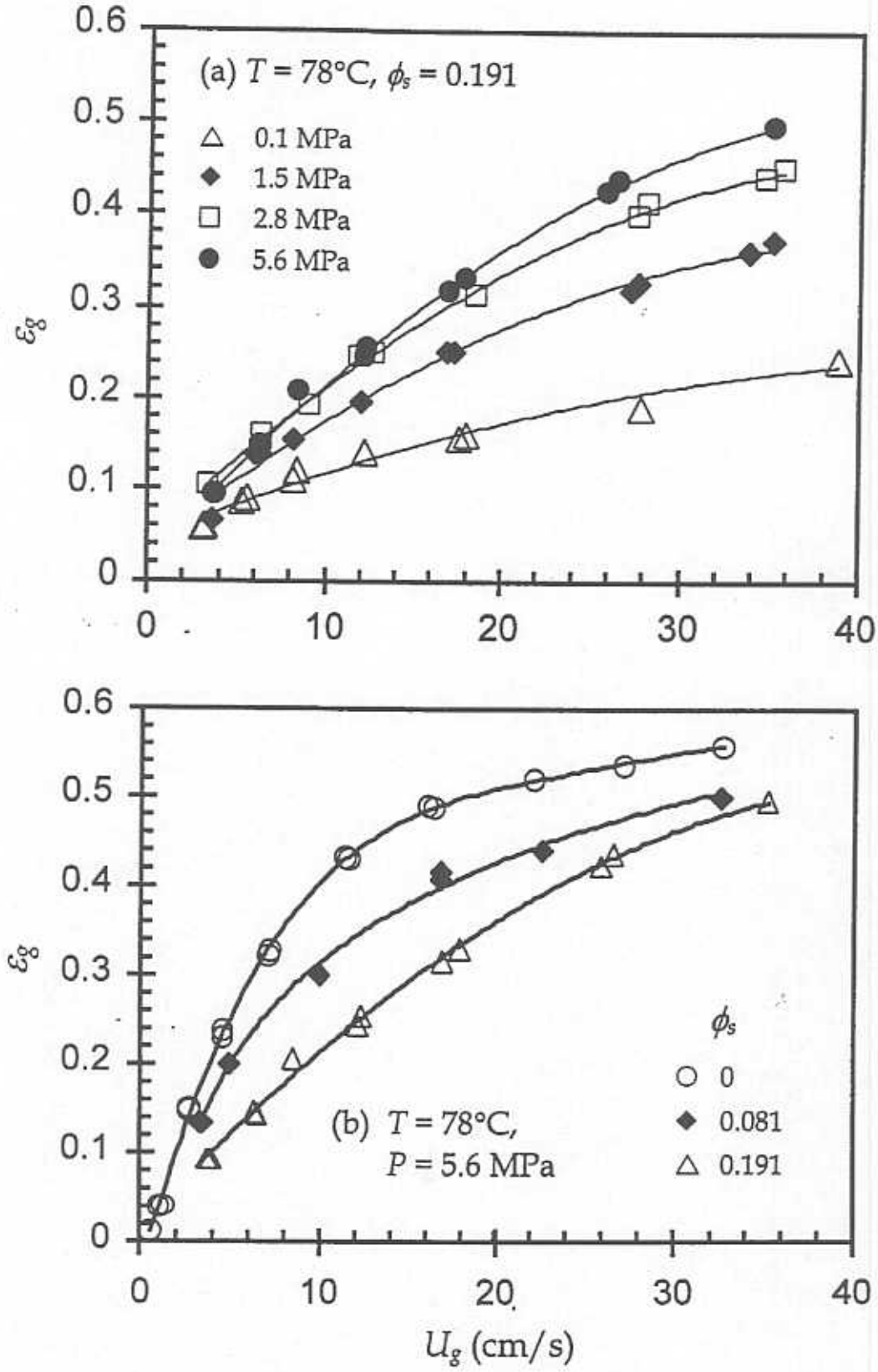
(a) T = 78°C, ϕ_s = 0.191
0.1 MPa
1.5 MPa
2.8 MPa
5.6 MPa
ε_g
0.6
0.5
0.4
0.3
0.2
0.1
0
0
10
20
30
40
(b) T = 78°C,
P = 5.6 MPa
ϕ_s
0
0.081
0.191
U_g (cm/s)

Figure 18

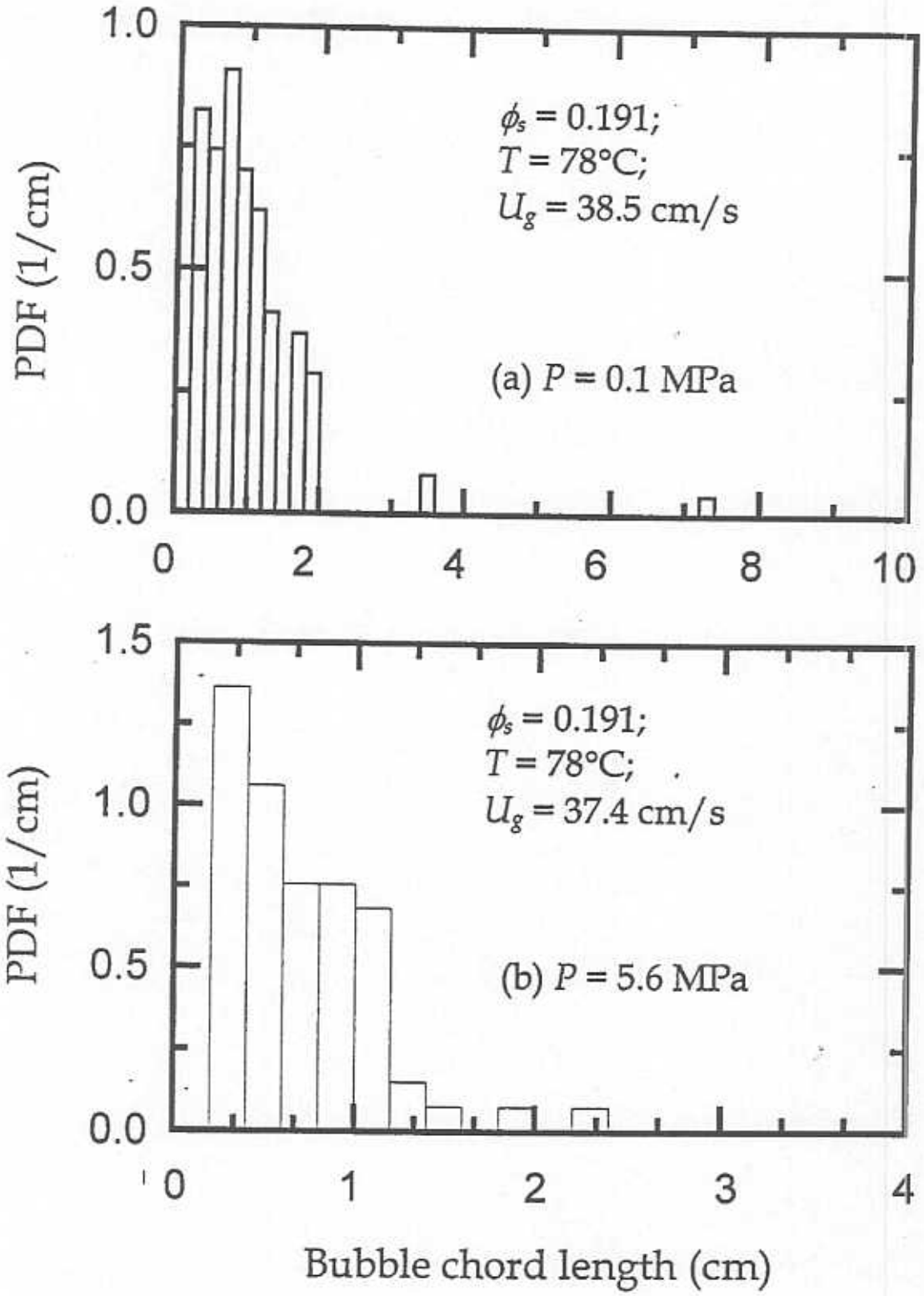
1.0
0.5
0.0
PDF (1/cm)
ϕ_s = 0.191;
T = 78°C;
U_g = 38.5 cm/s
(a) P = 0.1 MPa
0
2
4
6
8
10
1.5
1.0
0.5
0.0
PDF (1/cm)
ϕ_s = 0.191;
T = 78°C;
U_g = 37.4 cm/s
(b) P = 5.6 MPa
0
1
2
3
4
Bubble chord length (cm)

Figure 19

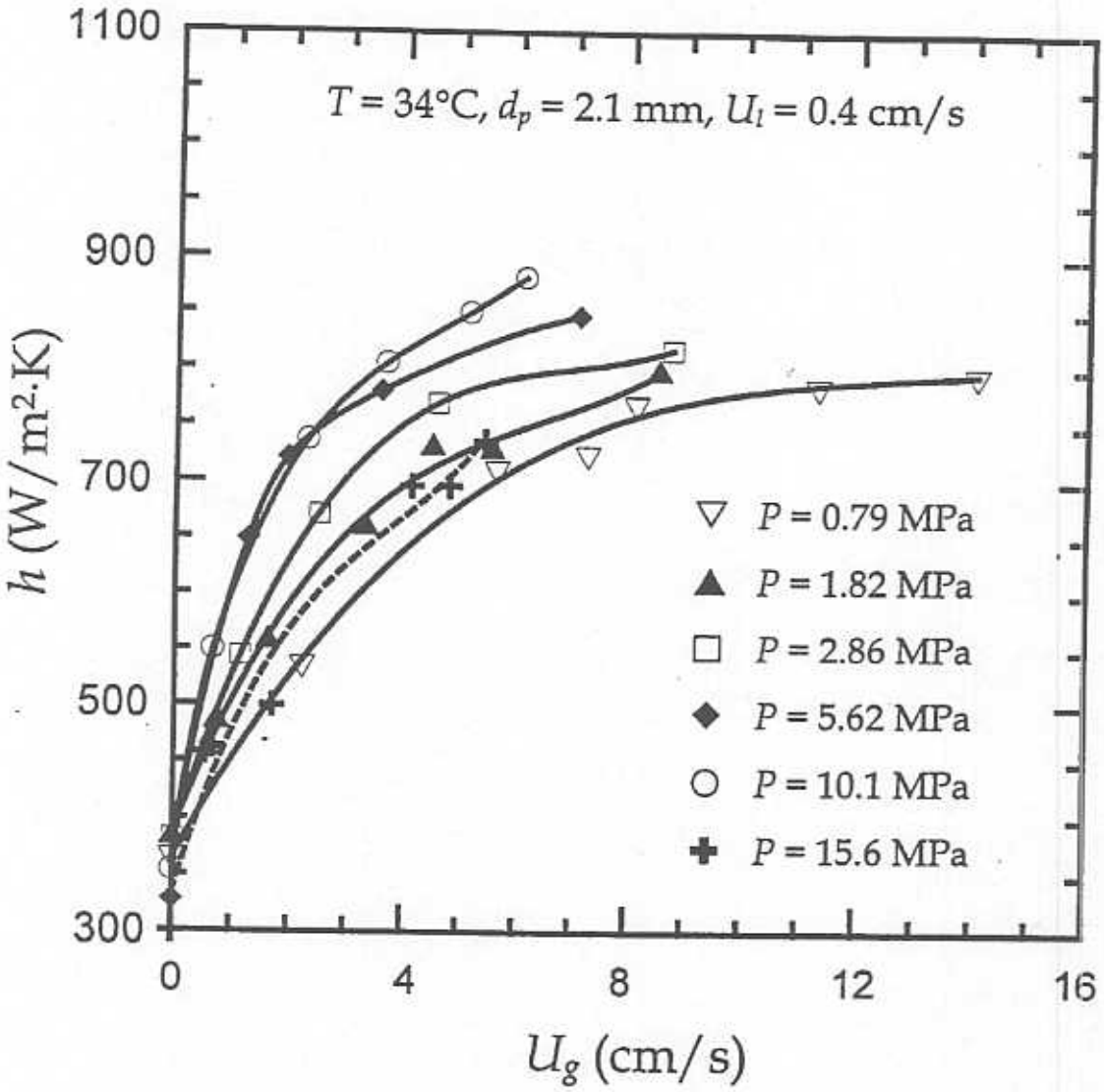
T = 34°C, d_p = 2.1 mm, U_l = 0.4 cm/s
h (W/m²·K)
1100
900
700
500
300
0
4
8
12
16
U_g (cm/s)
P = 0.79 MPa
P = 1.82 MPa
P = 2.86 MPa
P = 5.62 MPa
P = 10.1 MPa
P = 15.6 MPa

Figure 20

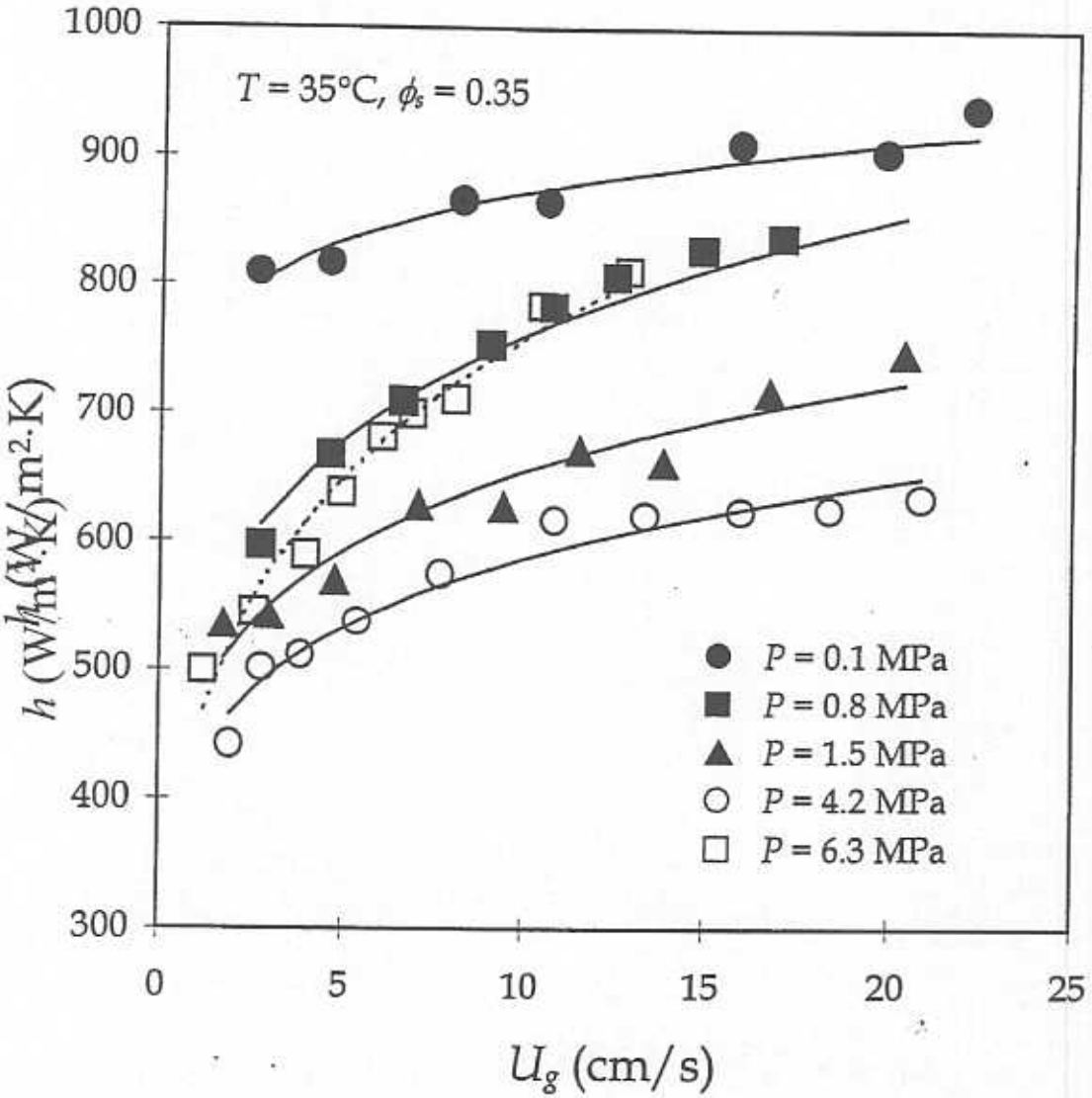
T = 35°C, ϕ_s = 0.35
h (W/m²·K)
U_g (cm/s)
P = 0.1 MPa
P = 0.8 MPa
P = 1.5 MPa
P = 4.2 MPa
P = 6.3 MPa
1000
900
800
700
600
500
400
300
0
5
10
15
20
25

Figure 21